Heliyon 10 (2024) e31707

Contents lists available at ScienceDirect

Heliyon

journal homepage: www.cell.com/heliyon

Research article

Identification of PANoptosis-related genes as prognostic indicators of thyroid cancer

Diya Xie [a], Liyong Huang [a,*], Cheng Li [a], Ruozhen Wu [b], Zhigang Zheng [a], Fengmin Liu [c], Huayong Cheng [a]

[a] Department of General Surgery, First General Hospital of Fuzhou Affiliated of Fujian Medical University, Fuzhou, Fujian Province, China
[b] Department of Gastrointestinal Surgery, First Affiliated Hospital of Fujian Medical University, Fuzhou, Fujian Province, China
[c] Department of Endocrinology, First General Hospital of Fuzhou Affiliated of Fujian Medical University, Fuzhou, Fujian Province, China

ARTICLE INFO

Keywords:
Thyroid cancer
PANoptosis-related genes
LASSO-Cox regression
Prognosis
TCGA
GEO

ABSTRACT

Background: Thyroid cancer (THCA) has become a common malignancy in recent years, with the mortality rate steadily increasing. PANoptosis is a unique kind of programmed cell death (PCD), including pyroptosis, necroptosis, and apoptosis, and is involved in the proliferation and prognosis of numerous cancers. This paper demonstrated the connection between PANoptosis-related genes and THCA based on the analyses of Gene Expression Omnibus (GEO) and The Cancer Genome Atlas (TCGA) databases, which have not been evaluated yet.

Methods: We identified PANoptosis-related differentially expressed genes (PRDEGs) by multi-analyzing the TCGA-THCA and GEO datasets. To identify the significant PRDEGs, a prognostic model was constructed using least absolute shrinkage and selection operator regression (LASSO). The predictive values of the significant PRDEGs for THCA outcomes were determined using Cox regression analysis and nomograms. Gene enrichment analyses were performed. Finally, immunohistochemistry was carried out using the human protein atlas.

Results: A LASSO regression model based on nine PRDEGs was constructed, and the prognostic value of key PRDEGs was explored via risk score. Univariate and multivariate Cox regression were implemented to identify further three significant PRDEGs closely related to distant metastasis, lymph node metastasis, and tumor stage. Then, a nomogram was constructed, which presented high predictive accuracy for 5 years survival of THCA patients. Gene enrichment analyses in THCA were strongly associated with PCD pathways. CASP6 presented significantly differential expression during clinical T stage, N stage, and PFI events ($P < 0.05$ for all) and demonstrated the highest degree of diagnostic efficacy in PRDEGs (HR: 2.060, 95 % CI: 1.170–3.628, $P < 0.05$). Immunohistochemistry showed CASP6 was more abundant in THCA tumor tissue.

Conclusion: A potential prognostic role for PRDEGs in THCA was identified, providing a new direction for treatment. CASP6 may be a potential therapeutic target and a novel prognostic biomarker for THCA.

Abbreviations: TCGA, the cancer genome atlas; THCA, thyroid cancer; PRGs, PANoptosis-related genes; PRDEGs, PANoptosis-related differentially expressed genes; GO, Gene Ontology; KEGG, Kyoto Encyclopedia of Genes and Genomes; GSEA, Gene Set Enrichment Analysis; GSVA, Gene Set Variation Analysis; PPI, Protein-protein interaction; LASSO, least absolute shrinkage and selection operator; ROC curve, receiver operating characteristic curve; IHC, immunohistochemical analysis; TPR, true positive rate; FPR, false positive rate; PFI, progression-free interval.

* Corresponding author. First General Hospital of Fuzhou Affiliated of Fujian Medical University, No. 190 Da Road, Taijiang District, Fuzhou, Fujian Province, 350004, China.

E-mail address: yanhuo@yyxxfh.wecom.work (L. Huang).

https://doi.org/10.1016/j.heliyon.2024.e31707
Received 8 April 2023; Received in revised form 24 April 2024; Accepted 21 May 2024
Available online 23 May 2024

1. Introduction

Thyroid cancer (THCA) is a common malignant tumor of the thyroid gland in the world, which accounts for approximately 1 % of entire malignancies [1]. Globally, the THCA morbidity rate has increased in recent decades and is estimated to be the fourth leading cancer type [2]. With the advances in treatment made, including surgical resection, radioactive iodine, thyroid-stimulating hormone (TSH)-suppressive therapy, redifferentiation drugs, targeted therapies, and immunotherapy [3], patients with papillary thyroid carcinomas have an overall 5-year survival of as high as 95 %. Despite this, recurrence and metastasis still occur frequently (20–30 %) [4], which results in increased mortality associated with sizeable social healthcare burdens [5]. About half of distant metastasis patients pass away within five years [6,7]. Hence, it is essential to identify a more accurate prognostic module for THCA to develop and introduce novel treatments.

Programmed cell death (PCD) is related to the occurrence and progression of malignancies and includes classical methods such as apoptosis, necroptosis, and pyroptosis. PANoptosis describes the simultaneous occurrence and regulation of apoptosis, necroptosis, and pyroptosis in the pathological processes of some diseases [8]. Plenty of evidence has been unveiled that PANoptosis participates in the development of cancer. A mouse model lacking IRF1 (an upstream regulator of PANoptosis) was found to be hypersusceptible to colorectal tumorigenesis [9]. Despite their resistance to the progression of melanoma and colorectal cancer, mice with adenosine deaminase acting on RNA-1 (ADAR1) deficiency exhibit restored tumorigenesis when the ZBP1 Zalpha2 domain is deleted, suggesting that ADAR1 restrains ZBP1-mediated PANoptosis, thereby facilitating tumorigenesis [10]. The PANscore, a scoring system based on PANoptosis patterns of individual gastric cancer patients, was developed, and the low PANscore group achieved higher immunotherapy response rates and prognoses. More recently, PANoptosis-related gene signatures for gliomas have been proven to be prognostic. However, to date, PANoptosis-related differentially expressed genes (PRDEGs) have not been established as prognostic biomarkers of THCA.

The goal of this research was to analyze PANoptosis-related genes in THCA using bioinformatics. The 510 THCA and 58 normal samples from The Cancer Genome Atlas (TCGA) database were utilized to acquire clinical data and gene expression. The GeneCards database was applied to download 14 PANoptosis-related genes. We screened the relevant literature in the PubMed database, resulting in 23 PANoptosis-related genes (PRGs). We then combined and de-duplicated the two resources, resulting in a final set of 28 PRGs, which were included in subsequent analyses. The GEO database was applied to acquire THCA gene expression data and clinical datasets (GSE33630, GSE35570, GSE65144, and GSE76039). We identified 14 TCGA-THCA PRDEGs that were consistent with those in the GSE33630 and GSE35570 datasets. According to the above data resources, a risk scoring system was constructed using the TCGA-THCA dataset and applied to a combined GEO dataset, including GSE33630, GSE35570, GSE65144, and GSE76039, to identify three PRDEGS. A nomogram was built by considering the three PRDEGs and then validated by calibration and decision curve analysis (DCA). In addition, the potential function and mechanism of PRDEGs in TCGA-THCA were explored by protein-protein interaction (PPI) network analysis, functional analysis, gene set variation analysis (GSVA), and gene set enrichment analysis (GSEA). As a result, three PRGs were discovered to be independent predictive factors of observed survival in THCA patients. CASP6 may be a potential therapeutic target and a prognostic biomarker for patients with THCA.

2. Materials & methods

2.1. Data download

With the application of the R package "TCGAbiolinks", the expression matrix of the THCA dataset was downloaded from TCGA (https://portal.gdc.cancer.gov/) [11], including 510 samples of THCA (tumor group) and 58 paracancerous samples (normal group), standardized as Fragments Per Kilobase per million; the UCSC Xena database (http://genome.ucsc.edu) was utilized to acquire the relevant clinical data [12]. R package “limma” was utilized to normalize the count sequencing data from TCGA-THCA [13]. R package GEOquery was utilized to acquire clinical information and THCA-related gene expression data from the GEO database in datasets GSE33630 [14,15], GSE35570 [16], GSE65144 [17], and GSE76039 [18,19]. Gene annotation was performed by means of the GPL570 Affymetrix Human Genome U133 Plus 2.0 (HG-U133_Plus_2) Array. All the samples included in this study were obtained from *Homo sapiens*. GSE33630 consisted of gene expression profile microarray data from 60 samples of THCA and 45 samples of normal tissue. GSE33570 contains gene expression profile microarray data of 65 THCA tissue specimens and 51 normal tissue samples. The GSE65144 included 12 THCA samples and 13 normal thyroid tissue samples. Similarly, GSE76039 comprises 37 tumor tissue specimens. GSE33630 [20,21], GSE35570, GSE65144, and GSE76039 [22] served as validation sets.

The GeneCards database [23] (https://www.genecards.org/) provides concise genomic information on all known human genes. "PANoptosis" served as a keyword to search for PRGs (PANoptosis-related genes) in the GeneCards database, from which 14 PRGs were obtained. We also identified 23 PRGs by retrieving all relevant published literature [24,25] from PubMed. The PRGs from the two resources were further combined and deduplicated, resulting in a final set of 28 PRGs, which were used for subsequent analyses. The specific gene names are presented in Supplementary Table S1.

2.2. Differential expression analysis

To identify potential mechanisms, related biological features, and signaling pathways of differential genes between the tumor and normal groups in THCA datasets of TCGA, GSE33630, and GSE35570 were standardized using the R package "limma", followed by a

differential analysis of gene expression profiles between the two TCGA-THCA groups. The identification of differentially expressed genes (DEGs) was performed in diverse groups, with adjusted $P < 0.05$ and logFC >0.2 (upregulated genes) or < 0.2 (downregulated genes) as differential expression. R package "ggplot 2" was utilized to make volcano plots for DEG. Upregulated genes and downregulated genes were intersected with PRGs and displayed using Venn Diagrams. PRDEGs for THCA were derived by combining both intersections. Furthermore, we drew boxplots of group comparisons separately for DEGs in datasets including TCGA-THCA, GSE33630, and GSE35570. The DEGs with the same expression trend and statistically significant discrepancy were extracted for subsequent analyses, and their expression in TCGA-THCA dataset was plotted as a heatmap using the "pheatmap" package of R.

2.3. Gene Ontology (GO) and Kyoto Encyclopedia of Genes and Genomes (KEGG) enrichment analyses

Large-scale functional enrichment research is commonly conducted using GO analysis [26], which comprising molecular functions (MF), biological processes (BP), and cellular components (CC). KEGG [27,28] is a comprehensive database that integrates biological pathways, genomics, medicines, and diseases. The "ClusterProfiler" R package was utilized to conduct KEGG and GO pathway enrichment analyses of PRDEGs, with thresholds set as FDR <0.2 and $P < 0.05$, followed by correcting *P*-value by means of the Benjamini–Hochberg (BH) method.

2.4. GSEA

We assessed gene distribution trends within a predefined gene set to identify genes contributing to phenotypes using GSEA. The enrichment analysis was processed in genes from the tumor and normal groups of TCGA-THCA using the R package "ClusterProfiler" (seed = 2020), repeated 1000 times, Min Size = 10 and Max Size = 500; the *P*-value was corrected by the BH method. The *MSigDB* database was applied to download the "c2. cp.v7.2. symbols" gene set, and significantly enriched functions were identified with FDR (q-value) < 0.25 and $P < 0.05$.

3. GSVA

GSVA [29] is a non-parametric, unsupervised approach in which expression matrixes of genes in different samples are converted to examine the transcriptome results related to gene set enrichment to assess whether there are enriched different pathways in various samples. The MSigDB database was applied to download a "h.all.v7.4. symbols.gmt" gene set, and GSVA was conducted on TCGA-THCA, with adjusted $P < 0.05$ as statistical difference, so as to explore the functional enrichment difference between the two groups.

3.1. PPI network

STRING [30] is a database used to search for interactions between known and predictive proteins. In this study, we conducted STRING to construct a PPI network related to candidate PRDEGs, with >0.400 as the minimum required interaction score. Protein complexes with specific biological functions can be identified by looking for densely connected regions in the PPI network. The maximal clique centrality (MCC) algorithm has been broadly applied to performance indicators in bioinformatics. Cytoscape [31] (version 3.9.1) was applied to perform PPI network visualization. GeneMANIA, a website used to predict genes that possess similar functions to the screened PRDEGs, was employed to construct an interaction network of candidate genes.

3.2. Least absolute shrinkage and selection operator (LASSO) regression model

To obtain a prognostic model of PRDEGs in THCA, with 10-fold cross-validation, we utilized LASSO [32,33] regression (seed = 2021). In addition, we ran 1000 repeats per period to prevent overfitting. LASSO regression is a type of linear regression that avoids overfitting and enhances the generalization capability of the refined model by imposing a penalty term ($\lambda \times$ absolute values of slopes) on the magnitude of the model coefficients. According to the LASSO regression model, risk factor graphs were drawn to depict the group and survival status of each tumor sample in accordance with the risk score.

$$\text{risk score} = \sum_i Coefficient\ (hub\ gene_i) * mRNA\ Expression\ (hub\ gene_i)$$

3.3. Cox regression model

For the purpose of assessing the prognostic value of PRDEGs in THCA, the expression of screened PRDEGs in the TCGA-THCA dataset was analyzed using multivariate Cox regression with the *P*-value threshold set to 0.1, and then the Cox regression model was built and presented in a forest plot. According to the results of the multivariate, a nomogram was constructed to individualize the predicted probability of 1-, 3-, and 5-year survivals. A calibration evaluation was performed on the accuracy and discriminative capacity of the nomogram. Calibration curves and nomograms were drawn using R package "rms". The clinical utility of these models was assessed with DCA. The R package "ggDCA" [34] was adopted to conduct DCA and evaluate the predictions of 1-, 3-, and 5-year prognostic nomograms.

3.4. Immunohistochemical analysis

Immunohistochemical (IHC) analysis uses the principle of specific antigen-antibody binding to detect and locate target antigens in cells and tissues, mainly with light microscopy. Human Protein Atlas (HPA) [35] database (www.proteinatlas.org/) was utilized to implement IHC analysis for key gene expression screened by the Cox model in THCA and normal thyroid tissues before contrast staining.

3.5. Statistical methods

R version 4.1.2 was adopted for statistical analysis and plotting, and continuous variables are described by mean ± standard deviation. Data between two continuous variable groups were compared using the Wilcoxon rank sum test; Student's *t*-test was utilized for statistical difference between the two groups, and the Kruskal–Wallis test was implemented for multi-group comparison. Categorical variables were examined by means of chi-square or Fisher's exact tests. LASSO regression was carried out using the "glmnet" [36] package, and R package "pROC" [37] was applied to generate a receiver operating characteristic (ROC) curve. Unless otherwise indicated, correlations were analyzed using the Spearman test, with statistical significance setting as two-tailed *P*-values less than 0.05.

4. Results

4.1. Differential expression analysis

Altogether, there were 18,436 DEGs acquired from the TCGA-THCA dataset, 10,798 of which were identified using the following thresholds: average $|\log FC| > 0.2$ and adjusted $P < 0.05$. Under such threshold, 5863 DEGs were highly expressed (upregulated), and 4935 DEGs were lowly expressed (downregulated) in THCA, as shown in Fig. 1. The final DEGs were visualized using a volcano plot (Fig. 2A). Eight upregulated genes (*CASP6*, *CASP7*, *FADD*, *GSDMD*, *MLKL*, *PSTPIP2*, *PYCARD*, and *RBCK1*) and six downregulated genes (*AIM2*, *IFNG*, *TAB3*, *TNF*, *TNFAIP3*, and *ZBP1*) were maintained by taking the intersection of diversely regulated DEGs and PRGs, and a Venn diagram was generated (Fig. 2B and C). The names and expression information for the 14 PRDEGs are listed in Tables 1 and 2. Next, we drew grouped comparison plots (Fig. 2D–F) of the 14 PRDEGs in TCGA-THCA, GSE 33630, and GSE35570 to recognize the expression trends and whether the differences were statistically significant. According to the figure, comparing genes in the GSE33630 and GSE35570 datasets with TCGA, nine genes were consistent with the validation results, including *CASP6*, *CASP7*, *FADD*, *GSDMD*, *MLKL*, *PSTPIP2*, *PYCARD*, *RBCK1*, and *TAB3*.

4.2. Heatmap and GOKEGG enrichment analysis

The expression of the nine PRDEGs in TCGA-THCA is depicted in a heatmap (Fig. 3A). To analyze the association between THCA and the BP, CC, and MF of nine PRDEGs (*CASP6*, *CASP7*, *FADD*, *GSDMD*, *MLKL*, *PSTPIP2*, *PYCARD*, *RBCK1*, and *TAB3*), we conducted

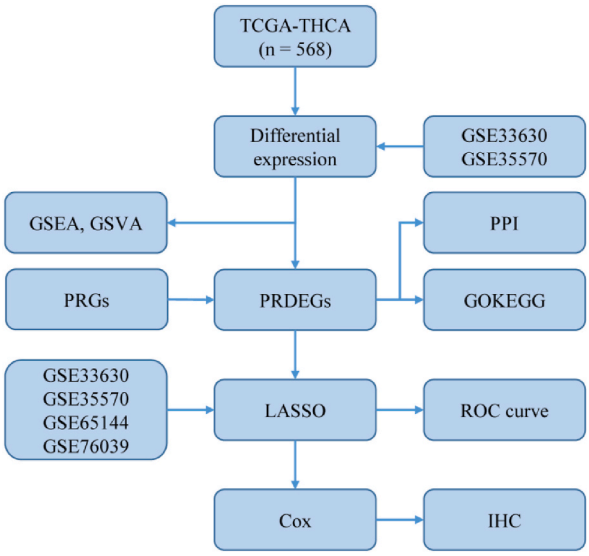

Fig. 1. Flowchart of the selection of the related genes. TCGA, the cancer genome atlas. THCA, thyroid cancer. PRGs, PANoptosis-related genes. PRDEGs, PANoptosis-related differentially expressed genes. GO, Gene Ontology. KEGG, Kyoto Encyclopedia of Genes and Genomes. GSEA, Gene Set Enrichment Analysis. GSVA, Gene Set Variation Analysis. PPI, Protein-protein interaction. LASSO, least absolute shrinkage and selection operator. ROC curve, receiver operating characteristic curve. IHC, immunohistochemical analysis.

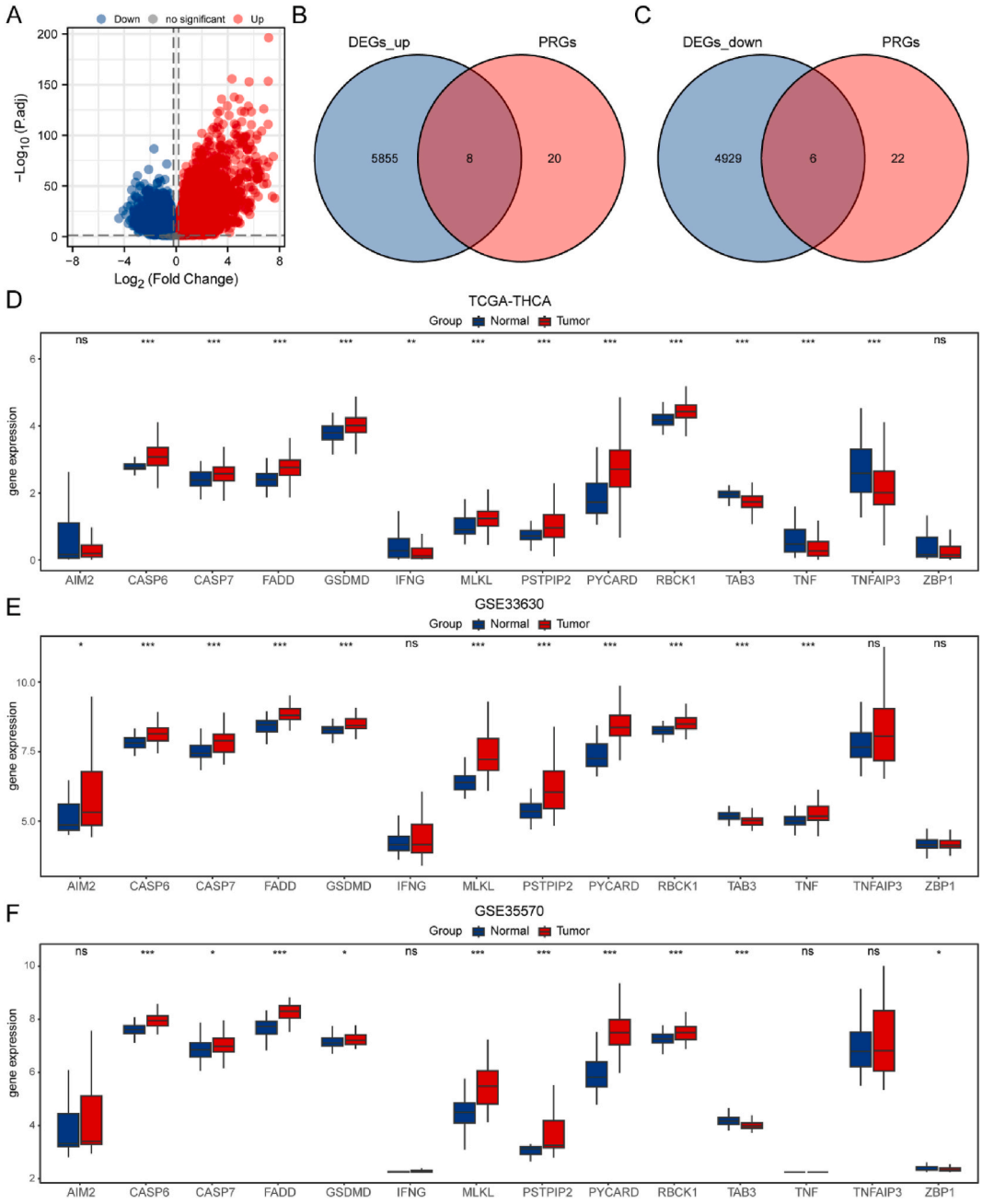

Fig. 2. Analyses of differentially expressed genes. (A) Volcano plot of the distribution of all differentially expressed genes, mapping 5863 upregulated (red dots) and 4935 downregulated (blue dots) genes. (B) Venn diagram showing overlap of the upregulated DEGs and the PRGs. (C) Venn diagram showing overlap of the downregulated DEGs and the PRGs. (D–E) Expression differences in the 14 PRDEGs between tumor tissues and normal samples in TCGA-THCA, GSE33630, and GSE35570 datasets. Ns, not significant, $P \geq 0.05$; *, $P < 0.05$; **, $P < 0.01$; ***, $P < 0.001$. TCGA, the cancer genome atlas. THCA, thyroid cancer. DEGs, differentially expressed genes. PRGs, PANoptosis-related genes. PRDEGs, PANoptosis-related differentially expressed genes. (For interpretation of the references to color in this figure legend, the reader is referred to the Web version of this article.)

GOKEGG gene function enrichment analysis (Table 3) of the PRDEGs, with a threshold of FDR (q-value) < 0.2 and $P < 0.05$. According to GO enrichment analysis, the genes in BP were mainly enriched in the "necroptotic process" (GO:0070,266), "programmed necrotic cell death" (GO:0097,300), and "positive regulation of extrinsic apoptotic signaling pathway" (GO:2,001,238), while in CC, mainly involved "inflammasome complex" (GO:0061,702), "cytosolic part" (GO:0044,445), "secretory granule lumen" (GO:0034,774), and MF primarily engaged in "cysteine-type endopeptidase activity involved in the apoptotic process" (GO:0097,153), "cysteine-type

Table 1
List of gene symbol of PRDEGs.

Gene symbol				
AIM2	FADD	MLKL	RBCK1	TNFAIP3
CASP6	GSDMD	PSTPIP2	TAB3	ZBP1
CASP7	IFNG	PYCARD	TNF	

PRDEGs, PANoptosis-related differentially expressed genes.

Table 2
Expression difference in PRDEGs.

Gene Symbol	logFC	*P*-value	adj.P
AIM2	−1.419186732	$5.32e^{-07}$	$2.11e^{-06}$
CASP6	0.452419353	$9.72e^{-16}$	$9.81e^{-15}$
CASP7	0.254072692	$1.11e^{-05}$	$3.68e^{-05}$
FADD	0.475491767	$1.85e^{-16}$	$2.00e^{-15}$
GSDMD	0.283371728	$3.76e^{-05}$	0.000115305
IFNG	−0.87403605	0.003869742	0.008406309
MLKL	0.358276507	$8.54e^{-05}$	0.00024785
PSTPIP2	0.691976548	$2.11e^{-07}$	$8.82e^{-07}$
PYCARD	0.851316867	$3.10e^{-09}$	$1.61e^{-08}$
RBCK1	0.385396769	$3.44e^{-15}$	$3.29e^{-14}$
TAB3	−0.217431728	0.000114563	0.000326124
TNF	−0.60882139	0.009131725	0.018355204
TNFAIP3	−0.881702017	$3.48e^{-09}$	$1.79e^{-08}$
ZBP1	−0.661708952	0.013610214	0.026403918

PRDEGs, PANoptosis-related differentially expressed genes.

endopeptidase activity" (GO:0008234) and "receptor serine/threonine kinase binding" (GO:0033,612). According to KEGG enrichment analysis, the nine PRDEGs were involved in "*Salmonella* infection"" (hsa05132), "NOD-like receptor signaling pathway" (hsa04621), and "TNF signaling pathway" (hsa04668). The findings of the enrichment analysis are shown in a bar plot (Fig. 3B) and network diagram (Fig. 3C). Furthermore, we performed logFC combined GOKEGG enrichment analysis for nine PRDEGs based on the enrichment analysis and calculated the z-score of each molecule using the logFC obtained from the differential analysis of the tumor and normal groups according to the nine PRDEGs in the TCGA-THCA dataset. A chord diagram (Fig. 3D) and circular plot (Fig. 3E) are shown for functional annotation of the enrichment analysis combined with logFC. The circular plot depicted that cysteine-type "endopeptidase activity involved in the apoptotic process" (GO:0097,153) was the significant upregulated BP while "*Salmonella* infection" (hsa05132) was the significant upregulated KEGG pathway.

4.3. GSEA and GSVA

To disclose the impact of gene expression levels on the discrepancy between the THCA and normal groups, this study analyzed all genes in the TCGA-THCA dataset using GSEA to identify the associations between their expressions and CC, BP, and MF (Fig. 4A). The enrichment significance levels were FDR (q-value) < 0.25 and $P < 0.05$. GSEA showed that genes in TCGA-THCA dataset were enriched in "senescence and autophagy in cancer" (Fig. 4B), "p53 downstream pathway" (Fig. 4C), "Focal adhesion" (Fig. 4D), and "Fatty acid omega-oxidation" (Fig. 4E) (Table 4). For the purpose of further investigating the difference in hallmark gene sets between normal and tumor groups, analyses of all TCGA-THCA gene expressions were studied with GSVA. GSVA revealed that 44 hallmark gene sets presented significant differences ($P < 0.05$, Fig. 5A, Table 6) between distinct groups. Moreover, 15 hallmark gene sets, which possessed significant differences ($P < 0.001$, Fig. 5B), were displayed in grouped comparisons as a boxplot, showing that genes were primarily enriched in pathways including "hallmark apoptosis", "hallmark epithelial-mesenchymal transition", "hallmark fatty acid metabolism", "hallmark glycolysis", and "hallmark hedgehog signaling".

4.4. PPI network

The PPI network of nine PRDEGs (*CASP6*, *CASP7*, *FADD*, *GSDMD*, *MLKL*, *PSTPIP2*, *PYCARD*, *RBCK1*, and *TAB3*) was established with the STRING database. A PPI network was established for the hub genes with 0.400 as the minimum required interaction score and was further visualized (Fig. 6A) using Cytoscape software. The findings displayed no gene-gene interaction between *PSTPIP2* and other genes. Besides, each of the others contained an interaction with at least one PRDEG, of which *MLKL* presented the most interactions with the five other PRDEGs, including *CASP7*, *FADD*, *GSDMD*, *RBCK1*, and *TAB3*. Subsequently, the scores of PRDEGs that interacted with other nodes in the PPI network were calculated by means of the maximal clique centrality (MMC) method. Fig. 6B was created with gradual color changes from red to yellow according to the score in descending order and showed that MLKL was the first score of the MCC algorithm. Specific score ranks of each gene are provided in Supplementary Table S2. Finally, we used GeneMANIA to predict and construct a gene-gene interaction network map (Fig. 6C) of genes that function similarly to the nine PRDEGs to observe their

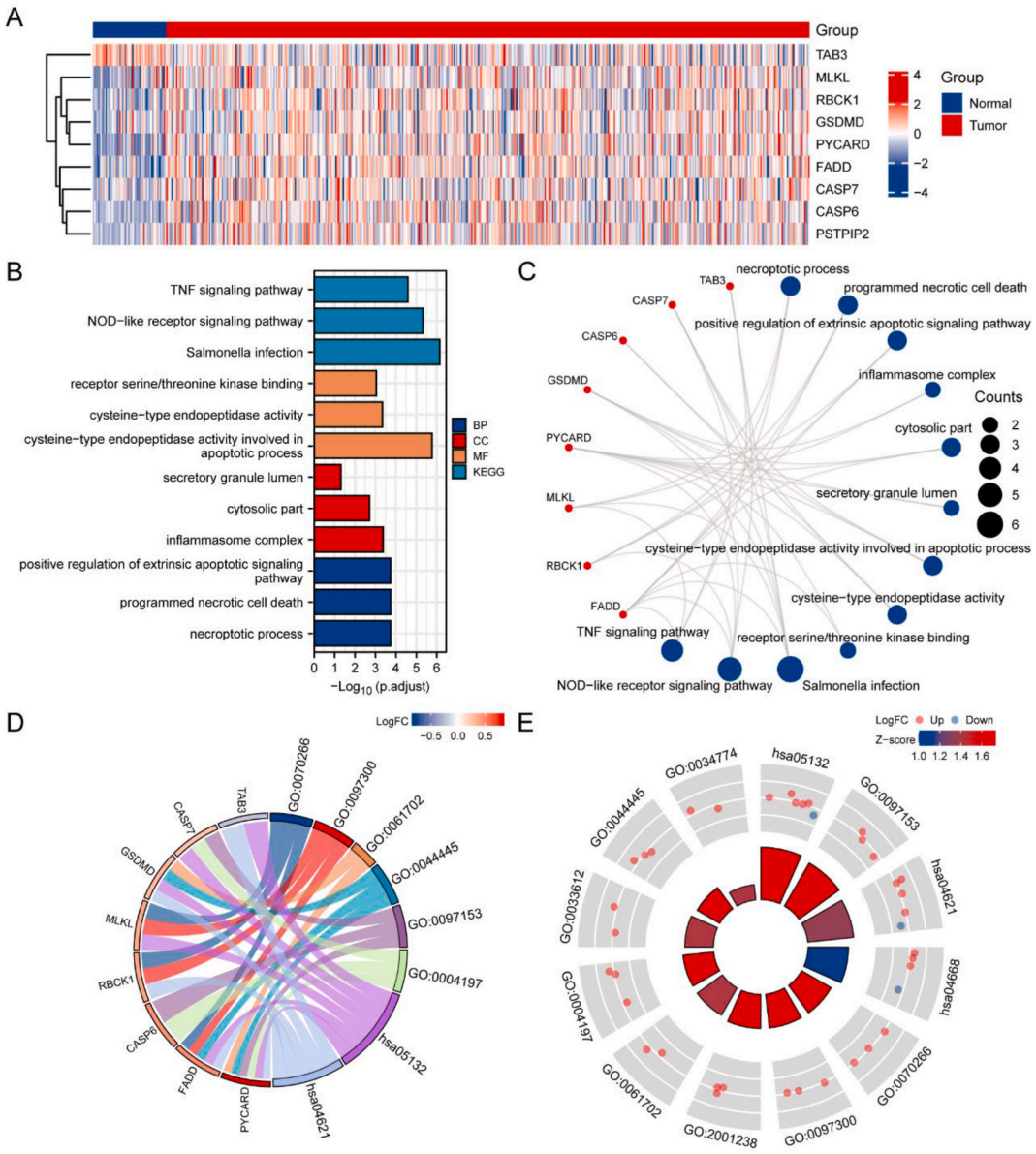

Fig. 3. Function and pathway enrichment analysis of PRDEGs. (A) Heatmap of expression patterns of nine PRDEGs in TCGA-THCA dataset. (B) Bar plot of significantly enriched GO annotations and KEGG pathway of the PRDEGs. (C) Network diagram of GO annotations and KEGG pathway: red dots for genes and blue dots for pathways. (D) Chord diagram of functional annotation of the PRDEGs combined with logFC using GO terms of biological processes and KEGG pathway. (E) Circular plot depicts the enriched GO and KEGG pathways of PRDEGs: red dots for upregulated genes (logFC > 0) and blue dots for downregulated genes (logFC < 0). GO, Gene Ontology. BP, biological process. CC, cellular component. MF, molecular function. KEGG, Kyoto Encyclopedia of Genes and Genomes. PRDEGs, PANoptosis-related differentially expressed genes. P < 0.05, and FDR (q. value) < 0.2 were set as the significant thresholds. (For interpretation of the references to color in this figure legend, the reader is referred to the Web version of this article.)

interaction, co-expression, and co-location.

4.5. LASSO regression model

The prognostic value of nine PRDEGs (*CASP6*, *CASP7*, *FADD*, *GSDMD*, *MLKL*, *PSTPIP2*, *PYCARD*, *RBCK1*, and *TAB3*) in the TCGA-THCA dataset was investigated using LASSO regression analysis (Fig. 7A and B). Normal samples were eliminated, and the median risk score was determined as a cutoff level, dividing tumor groups into high- and low-risk score groups. A risk score curve was utilized to visualize and display the results (Fig. 7C). The proportion of deaths in high-risk samples was higher than in low-risk samples.

Table 3
GOKEGG enrichment analysis results of PRDEGs.

ONTOLOGY	ID	Description	GeneRatio	BgRatio	*P*-value	p.adjust	q-value
BP	GO:0070,266	Necroptotic process	3/9	44/18,670	1.02e-[06]	1.81e^{-04}	5.00e^{-05}
BP	GO:0097,300	Programmed necrotic cell death	3/9	49/18,670	1.41e^{-06}	1.81e^{-04}	5.00e^{-05}
BP	GO:2,001,238	Positive regulation of extrinsic apoptotic signaling pathway	3/9	49/18,670	1.41e^{-06}	1.81e^{-04}	5.00e^{-05}
BP	GO:0070,265	Necrotic cell death	3/9	62/18,670	2.89e^{-06}	2.33e^{-04}	6.45e^{-05}
BP	GO:0043,122	Regulation of I-kappaB kinase/NF-kappaB signaling	4/9	237/18,670	3.03e^{-06}	2.33e^{-04}	6.45e^{-05}
CC	GO:0061,702	Inflammasome complex	2/9	14/19,717	1.68e^{-05}	4.20e^{-04}	2.48e^{-04}
CC	GO:0044,445	Cytosolic part	3/9	247/19,717	1.54e^{-04}	0.002	0.001
CC	GO:0034,774	Secretory granule lumen	2/9	321/19,717	0.009	0.049	0.029
CC	GO:0060,205	Cytoplasmic vesicle lumen	2/9	338/19,717	0.010	0.049	0.029
CC	GO:0031,983	Vesicle lumen	2/9	339/19,717	0.010	0.049	0.029
MF	GO:0097,153	Cysteine-type endopeptidase activity involved in apoptotic process	3/9	15/17,697	4.13e^{-08}	1.69e^{-06}	5.21e^{-07}
MF	GO:0004197	Cysteine-type endopeptidase activity	3/9	116/17,697	2.24e^{-05}	4.59e^{-04}	1.41e^{-04}
MF	GO:0033,612	Receptor serine/threonine kinase binding	2/9	25/17,697	6.86e^{-05}	9.09e^{-04}	2.80e^{-04}
MF	GO:0008234	Cysteine-type peptidase activity	3/9	184/17,697	8.87e^{-05}	9.09e^{-04}	2.80e^{-04}
MF	GO:0004175	Endopeptidase activity	3/9	427/17,697	0.001	0.009	0.003
KEGG	hsa05132	*Salmonella* infection	6/8	249/8076	2.15e^{-08}	7.10e^{-07}	4.53e^{-07}
KEGG	hsa04621	NOD-like receptor signaling pathway	5/8	181/8076	2.84e^{-07}	4.68e^{-06}	2.99e^{-06}
KEGG	hsa04668	TNF signaling pathway	4/8	112/8076	2.35e^{-06}	2.59e^{-05}	1.65e^{-05}
KEGG	hsa 04217	Necroptosis	4/8	159/8076	9.52e^{-06}	7.86e^{-05}	5.01e^{-05}
KEGG	hsa 05130	Pathogenic *Escherichia coli* infection	4/8	197/8076	2.23e^{-05}	1.47e^{-04}	9.38e^{-05}

GO, Gene Ontology. KEGG, Kyoto Encyclopedia of Genes and Genomes. PRDEGs, PANoptosis-related differentially expressed genes. BP, biological process. CC, cellular component. MF, molecular function.

Moreover, PRDEGs expression exhibited marked difference between the two groups in TCGA database, including the high expressions of *CASP6*, *CASP7*, *PSTPIP2*, *PYCARD*, *RBCK1*, and *TAB3* and the low expressions of *GSDMD* and *MLKL*. TCGA-THCA dataset was utilized to acquire the clinical data of patients with THCA, which were statistically analyzed (Table 5) to validate the LASSO regression model further. The combined dataset for validation was obtained by merging the datasets GSE33630, GSE35570, GSE65144, and GSE76039, and the LASSO model was conducted to determine median risk scores and distinguish the tumor group to groups with high- and low-risk scores. The expression of each PRDEG (*CASP6*, *CASP7*, *FADD*, *GSDMD*, *MLKL*, *PSTPIP2*, *PYCARD*, *RBCK1*, and *TAB3*) in TCGA-THCA dataset and the combined dataset were grouped by risk level and depicted as a group comparison map (Fig. 7D and E) to identify the trend of expression and whether there was statistically marked difference ($P < 0.05$). Finally, four genes were consistent between the combined dataset and TCGA-THCA dataset, namely *CASP6*, *GSDMD*, *MLKL*, and *RBCK1*.

4.6. Clinical correlation analysis

To research the connection between the expressions of four PRDEGs and the occurrence of THCA, we plotted ROC curves (Fig. 8A–D) of the above genes in the TCGA-THCA dataset by setting clinical status (tumor vs. normal) as the outcome variable. Both *CASP6* and *RBCK1* had the area under the curves (AUCs) larger than 0.7, indicating an accurate predictive ability of the tumor, whereas the AUCs of *GSDMD* and *MLKL* were more significant than 0.6 and less than 0.7, respectively, implying a lower accuracy of predictive power. In addition, we distinguished subgroups in patients with THCA based on M0 and M1 in clinical M stages, from which we produced a ROC curve of PRDEGs (Fig. 8E and F). The AUC value of RBCK1, between 0.6 and 0.7, suggested that the predictive ability of the outcome of M0 or M1 was low. We also plotted ROC curves (Fig. 8G and H) for the groups with high- and low-risk scores from the LASSO model as outcome variables. From the plot, the AUC value of *CASP6* was more significant than 0.8, illustrating a prognostic capacity for high- and low-risk outcomes. The AUC of *MLKL* was more significant than 0.6 and lower than 0.7; hence, the ability to predict high- and low-risk outcomes had low accuracy. Finally, clinical-related analyses of four PRDEGs were performed in T stage, N stage, M stage, and progression-free interval (PFI) subgroups (Fig. 8I-L), identified that the expression of *CASP6* was significantly different between T1&T2 and T3& T4 ($P < 0.01$) in clinical T stage, between N0 and N1 ($P < 0.001$) in clinical N stage, as well as between live and dead PFI events ($P < 0.05$). In addition, the expression of *MLKL* was different ($P < 0.01$) between M0 and M1 in the clinical M stage.

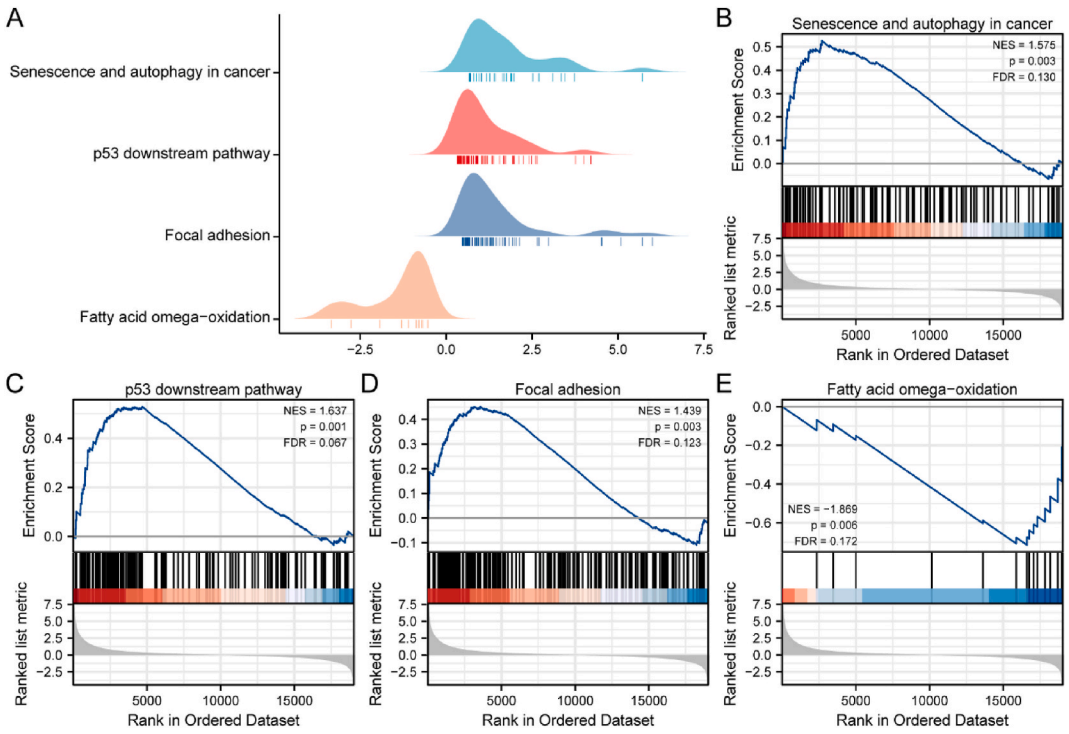

Fig. 4. Enrichment plots from GSEA in TCGA-THCA. Several biological processes and pathways are differentially enriched in TCGA-THCA (A), including the senescence and autophagy in cancer (B), p53 downstream pathway (C), focal adhesion (D), and fatty acid omega-oxidation (E). GSEA, Gene Set Enrichment Analysis. P < 0.05, and FDR (q.value) < 0.25 set as the significant thresholds.

4.7. Cox model

To validate the LASSO regression prognostic model, the correlation between the expression of four PRDEGs and clinical prognosis was explored through univariate and multivariate Cox regression analyses in the TCGA-THCA dataset, and a forest plot was drawn (Fig. 9A). Three PRDEGs (*CASP6*, *MLKL*, and *RBCK1*) exhibited a marked association between clinical outcome and expression (Table 7). Based on this, the prognostic power of multivariate Cox regression was assessed using a clinical prognostic nomogram model (Fig. 9B). We subsequently drew a calibration curve (Fig. 9C–E) on the calibration analysis of predictions of 1-, 3-, and 5-year survivals to assess the nomogram accuracy. The prediction (blue line) mainly corresponded to the ideal line (gray line) in the 5-year survival curve, which meant that in this model, the ability of 5-year prediction was better than the 1-year and 3-year. DCA (Fig. 9F–H) was applied to assess the clinical utility of 1-, 3-, and 5-year LASSO-Cox regression models and demonstrated that the model provides a more accurate 5-year prediction than the 1-year and 3-year models.

4.8. Immunohistochemical analysis

In the multivariate Cox model, with the hazard ratio (HR) of *CASP6* higher than 1, its expression in THCA tissues and normal thyroid tissues was further demonstrated by immunohistochemical analysis in the HPA dataset with the HPA024303 antibody. *CASP6* was more abundant in THCA tumor tissue (Fig. 10B) than in normal thyroid tissue (Fig. 10A).

5. Discussion

Thyroid cancer (THCA) is defined as a tumor with a better prognosis. Up to 90 % of THCAs are well differentiated and have a favorable prognosis [38,39] under traditional clinical treatment, including surgery, radioactive iodine, and endocrine suppression therapy. Nevertheless, 20–30 % of patients still face tumor recrudescence, resistance to radioactive iodine treatment, and distant metastasis, yielding poor prognosis and shorter survival [40], suggesting that the classical prognostic method based on clinicopathological risk is not sufficient.

Programmed cell death (PCD) plays a crucial role in tumorigenesis. Several studies have recently identified a unique form of inflammatory PCD, namely PANoptosis, which is controlled by PANoptosomes composed of multifaceted subunits that are the assembly of incorporating pivotal components of other PCD pathways, including necroptosis, apoptosis, and pyroptosis [41]. A single PCD pathway alone cannot account for the biological effects observed in PANoptosis [42]. Triggering PANoptosis may elicit extensive responses to kill an abundant variety of cancer cells while simultaneously arousing lasting immune protection, initiating robust

Table 4
GSEA analysis of the TCGA-THCA dataset.

Description	setSize	enrichmentScore	NES	*P*-value	p.adjust	q-value
REACTOME_FORMATION_OF_THE_CORNIFIED_ENVELOPE	128	0.70590884	2.16973083	0.00114155	0.0708692	0.06733117
REACTOME_COLLAGEN_DEGRADATION	64	0.75265778	2.12182827	0.00128866	0.0708692	0.06733117
REACTOME_DEGRADATION_OF_THE_EXTRACELLULAR_MATRIX	140	0.6796979	2.1065108	0.00113379	0.0708692	0.06733117
REACTOME_KERATINIZATION	216	0.63214431	2.03185018	0.00104932	0.0708692	0.06733117
REACTOME_ACTIVATION_OF_MATRIX_METALLOPROTEINASES	33	0.77740605	2.00009345	0.00133869	0.0708692	0.06733117
PID_INTEGRIN1_PATHWAY	66	0.6904069	1.9570183	0.00126904	0.0708692	0.06733117
REACTOME_CELL_JUNCTION_ORGANIZATION	91	0.65718076	1.95167563	0.0011976	0.0708692	0.06733117
REACTOME_EXTRACELLULAR_MATRIX_ORGANIZATION	300	0.5961427	1.94142062	0.00104058	0.0708692	0.06733117
REACTOME_COLLAGEN_FORMATION	90	0.65653842	1.94106179	0.00120482	0.0708692	0.06733117
REACTOME_SYNDECAN_INTERACTIONS	27	0.78546485	1.9330673	0.00140056	0.0708692	0.06733117
PID_SYNDECAN_1_PATHWAY	46	0.70776478	1.91319355	0.00133156	0.0708692	0.06733117
NABA_ECM_REGULATORS	237	0.58937386	1.89552421	0.00104822	0.0708692	0.06733117
REACTOME_CELL_CELL_JUNCTION_ORGANIZATION	64	0.66849329	1.88455897	0.00128866	0.0708692	0.06733117
REACTOME_INTEGRIN_CELL_SURFACE_INTERACTIONS	84	0.63154824	1.85889626	0.00121359	0.0708692	0.06733117
REACTOME_ADHERENS_JUNCTIONS_INTERACTIONS	33	0.72028962	1.85314553	0.00133869	0.0708692	0.06733117
REACTOME_REGULATION_OF_TLR_BY_ENDOGENOUS_LIGAND	19	0.80298603	1.84646543	0.00143472	0.0708692	0.06733117
PID_TAP63_PATHWAY	53	0.66582091	1.84059312	0.00130378	0.0708692	0.06733117
REACTOME_NON_INTEGRIN_MEMBRANE_ECM_INTERACTIONS	59	0.6565379	1.83548998	0.00131234	0.0708692	0.06733117
PID_AVB3_INTEGRIN_PATHWAY	74	0.63446547	1.83257655	0.00124533	0.0708692	0.06733117
REACTOME_DISEASES_ASSOCIATED_WITH_O_GLYCOSYLATION_OF_PROTEINS	67	0.64096343	1.82107843	0.00126263	0.0708692	0.06733117
REACTOME_CELL_CELL_COMMUNICATION	129	0.59063944	1.81573801	0.00114155	0.0708692	0.06733117
REACTOME_MET_ACTIVATES_PTK2_SIGNALING	30	0.7124567	1.8022331	0.0013624	0.0708692	0.06733117
REACTOME_MET_PROMOTES_CELL_MOTILITY	41	0.67301382	1.79422414	0.00133156	0.0708692	0.06733117
REACTOME_DISEASES_ASSOCIATED_WITH_SURFACTANT_METABOLISM	10	0.89882431	1.78864192	0.00312989	0.12963368	0.12316192
REACTOME_O_LINKED_GLYCOSYLATION	110	0.59281552	1.78792773	0.00117647	0.0708692	0.06733117
PID_INTEGRIN3_PATHWAY	43	0.66523744	1.78768891	0.0013245	0.0708692	0.06733117
PID_P53_DOWNSTREAM_PATHWAY	136	0.52933552	1.63735221	0.00113250	0.07086920	0.06733116
WP_SENESCENCE_AND_AUTOPHAGY_IN_CANCER	105	0.52563855	1.57457776	0.00356718	0.13641594	0.12960559
KEGG_FOCAL_ADHESION	199	0.45188839	1.43906629	0.00320855	0.12963368	0.12316192
WP_FATTY_ACID_OMEGA_OXIDATION	15	−0.7143672	−1.8693513	0.00604229	0.18134536	0.17229198

GSEA, Gene Set Enrichment Analysis. TCGA, the cancer genome atlas. THCA, thyroid cancer.

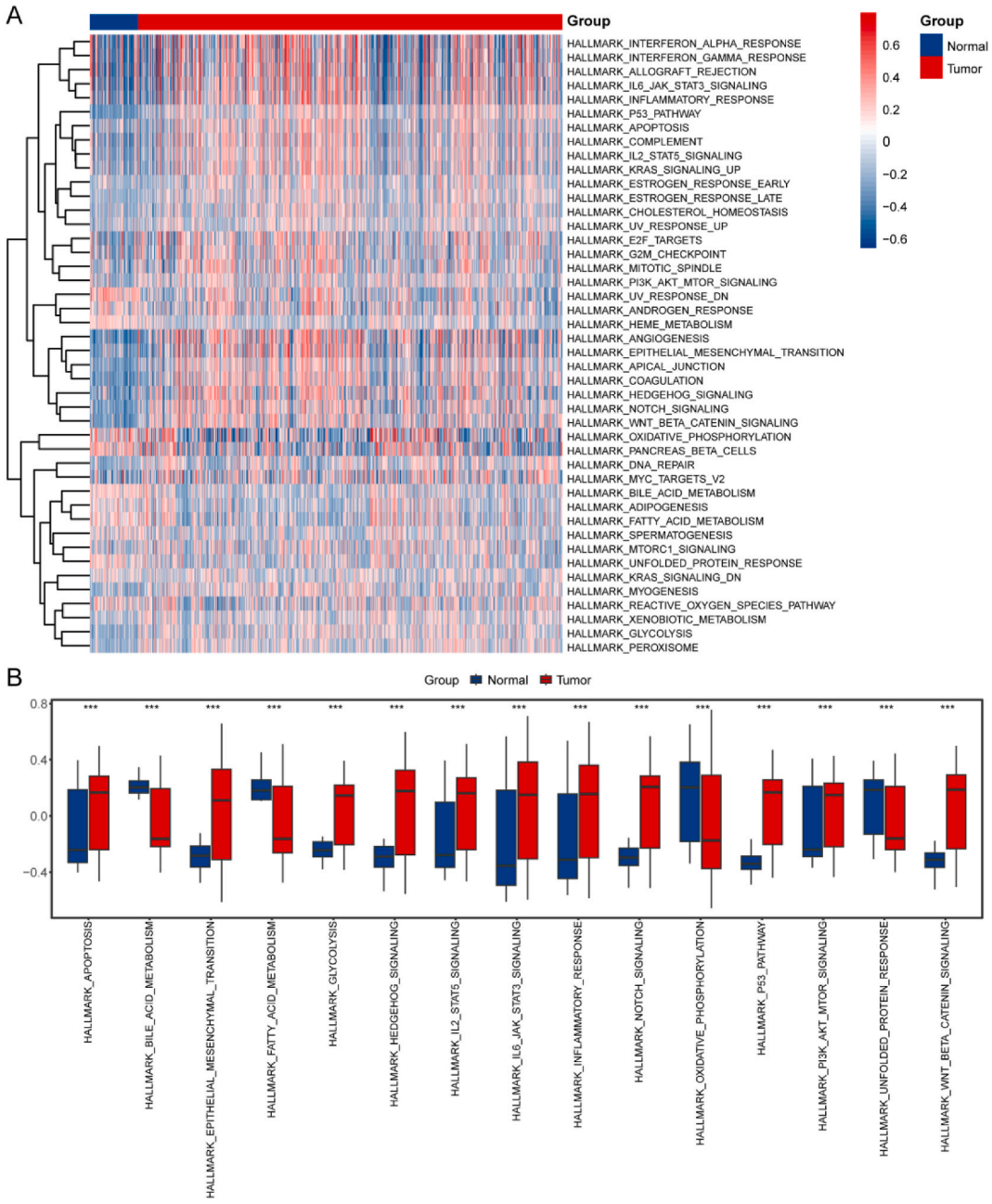

Fig. 5. GSVA of TCGA-THCA. (A) Heatmap of enrichment on hallmark gene sets from GSVA in TCGA-THCA. (B) Boxplot shows differences in 15 statistically significant hallmark gene sets between THCA and normal groups based on GSVA. ***, $P < 0.001$. GSVA, Gene Set Variation Analysis.

inflammatory cell death, and enhancing the function and durability of T cells in tumor microenvironments [9].

The presence of PRDEGs has been reported as a prognostic marker in multiple tumors such as melanoma [10] and gastric carcinoma [43]. However, research on the potential biomarkers of THCA in PANoptosis genes is limited. This is the first research to examine the prognostic role of PRDEGs in THCA. We not only constructed a prognostic model using nine PRDEGs but also identified three PRDEGs as biomarkers for THCA.

Based on the TCGA database, this study developed a prognostic model of THCA survival using nine PRGs: *CASP6*, *CASP7*, *FADD*, *GSDMD*, *MLKL*, *PSTPIP2*, *PYCARD*, *RBCK1*, and *TAB3*. Specifically, a nomogram model that includes *CASP6*, *MLKL*, and *RBCK1* may be a feasible tool for predicting the probability of survival in patients with THCA. Each gene in the model showed significant functions in diverse tumor statuses. In addition, a gene-based nomogram was constructed, which may have an accurate prediction of the 5-year survival probability of THCA. *CASP6* expression had a significant association with the prognosis of THCA, and its higher expression

Table 5
Characteristics of patients with THCA in the TCGA datasets.

Characteristic	levels	Overall
n		510
T stage, n (%)	T1	143 (28.1 %)
	T2	167 (32.9 %)
	T3	175 (34.4 %)
	T4	23 (4.5 %)
N stage, n (%)	N0	229 (49.8 %)
	N1	231 (50.2 %)
M stage, n (%)	M0	286 (96.9 %)
	M1	9 (3.1 %)
Pathologic stage, n (%)	Stage I	286 (56.3 %)
	Stage II	52 (10.2 %)
	Stage III	113 (22.2 %)
	Stage IV	57 (11.2 %)
Gender, n (%)	Female	371 (72.7 %)
	Male	139 (27.3 %)
Age, n (%)	≤45	241 (47.3 %)
	>45	269 (52.7 %)
OS event, n (%)	Alive	494 (96.9 %)
	Dead	16 (3.1 %)
PFI event, n (%)	Alive	456 (89.4 %)
	Dead	54 (10.6 %)
Age, median (IQR)		46 (35, 58)

THCA, thyroid cancer. TCGA, the cancer genome atlas. OS, overall survival. PFI, progression-free interval. IQR, interquartile range.

had a correlation with a marked reduction of progression-free survival. Furthermore, in THCA, *CASP6* expression had a noticeable correlation with lymph node metastasis and tumor stage.

TGF-β activated kinase 1 (TAK1) binding protein 3 (*TAB3*) activates nuclear factor-κB by linking TAK1 to signaling molecules that function in the NF-κB signal transduction pathway. Knockdown *TAB3* reduced the expressions of the NF-κB pathway in human esophageal squamous carcinoma cells and inhibited the invasion, migration, and proliferation [44]. Criollo et al. confirmed that overexpression of *TAB3* suppresses autophagy, whereas its depletion triggers autophagy [45]. Furthermore, in response to TAK1 deficiency, multifaceted inflammatory cell death is caused by PANoptosome formation, which facilitates activation and pyroptosis of *NLRP3* inflammasome, *MLKL* (mixed lineage kinase domain-like)-mediated necroptosis, and *FADD*-caspase-8 dependent apoptosis [46]. In our study, the downregulation of *TAB3* in THCA may weaken the function of TAK1 to initiate PNAoptosis by *FADD*- and *MLKL*-upregulation and serve as a defensive factor against tumorigenesis. Furthermore, during TAK1 suppression induced by Yersinia infection, inflammatory caspases cleave gasdermin-D *(GSDMD)* is activated to induce cell death [47]. *GSDMD*, the executor of pyroptotic cell death, which is vital for host defense and the danger response. Through oligomerization of the *GSDMD N*-terminus, pores can be formed inside the cell membranes, which facilitates the release of pro-inflammatory cytokines, in turn leading to cell death [42]. Similar to GSDMD in pyroptosis, phosphorylation of *MLKL* induces self-oligomerization, forms pores within the plasma membranes, and lyses the cells [48]. The present study also demonstrated that *MLKL* expression had an association with the lower M stage and played a protective role in the THCA nomogram model. Caspase-7, an apoptotic executioner, which executes apoptosis by cleaving other substrates [49]. The above results are consistent with the conclusions of our study and imply the formation of *TAB3*-initiated PANoptosis, composed of caspase-7- and *FADD*-related apoptosis, *MLKL*-mediated necroptosis, and *GSDMD*-executed pyroptosis. Proline-serine-threoninephosphatase-interacting protein 2 (PSTPIP2) modulates F-actin bundling and facilitates the formation of filopodia, strongly indicating that this protein is involved in cancer invasion [50,51]. *PYCARD* is constituted of a pyrin domain (PYD) and a caspase activation and recruitment domain (CARD) [52,53]. *PYCARD* has diverse functions in many types of human tumors, including late-stage lung, gastric, and pancreatic cancers [54–56]. A similar higher expression pattern was observed in THCA for *PSTPIP2* and *PYCARD* in our study. RBCK1 protein could serve as an applicable diagnostic signature and drug target due to its abnormal expression in breast tumors. Research has shown that *RBCK1* modulates breast cancer progression through estrogen signaling pathways [57,58]. Moreover, the *RBCK1* has been linked to unfavorable prognosis and endocrine resistance in breast cancer [59]. As THCA is one of the most prevalent endocrine tumors, our THCA model also showed that *RBCK1* is expressed more in the high-risk group.

Caspases are cysteine proteases that have crucial roles in apoptotic cell death. The activation of caspase 6 is an early event of apoptosis through proteolysis of lamin B, which induces apoptosis in human fetal thyroid cells (TAD-2) [60]. *CASP6* has generally been considered an apoptosis executor. Additionally, during infection with the influenza A virus (IAV), *CASP6* knockout macrophages showed a reduction in pyroptosis, demonstrating that it works in this process [61]. A prognostic model for glioma was constructed, in which *CASP6* showed higher expression in a high-risk group and had a close correlation with the anticancer drug nelarabine, indicating that *CASP6* may be involved in pan-cancer signaling pathways and influence the effectiveness of anticancer agents [62]. Moreover, the former study confirmed that *CASP6* promotes the interaction between *RIPK3* and ZBP1 through the *RHIM* (RIP homotypic interaction motif), enhancing ZBP1-triggered inflammasome activation, PANoptotic cell demise, and host defense mechanisms [63]. However, a

Table 6
GSVA analysis of the TCGA-THCA dataset.

ontology	logFC	Avenir	t	*P*-value	adj.P
HALLMARK_P53_PATHWAY	0.36295	0.012729	10.86072	$3.79e^{-25}$	$1.89e^{-23}$
ELECTROCOAGULATION	0.350964	0.020324	8.961907	$4.31e^{-18}$	$7.50e^{-17}$
HALLMARK_NOTCH_SIGNALING	0.343766	0.030524	8.956358	$4.50e^{-18}$	$7.50e^{-17}$
HALLMARK_WNT_BETA_CATENIN_SIGNALING	0.338027	0.013214	8.826929	$1.26e^{-17}$	$1.57e^{-16}$
HALLMARK_APICAL_JUNCTION	0.314673	0.014636	8.590547	$7.94e^{-17}$	$7.94e^{-16}$
LYMPHANGIOGENESIS	0.388934	0.019353	8.062906	$4.25e^{-15}$	$3.55e^{-14}$
HALLMARK_UV_RESPONSE_DN	−0.2586	0.003803	−6.81355	$2.38e^{-11}$	$1.70e^{-10}$
HALLMARK_GLYCOLYSIS	0.209504	−0.00232	6.748355	$3.62e^{-11}$	$2.26e^{-10}$
HALLMARK_HEME_METABOLISM	−0.19046	0.001482	−6.65432	$6.58e^{-11}$	$3.65e^{-10}$
HALLMARK_PEROXISOME	0.198578	0.001942	6.589468	$9.89e^{-11}$	$4.95e^{-10}$
HALLMARK_BILE_ACID_METABOLISM	−0.19416	−0.00903	−6.36022	$4.08e^{-10}$	$1.85e^{-09}$
HALLMARK_HEDGEHOG_SIGNALING	0.257311	0.007462	5.903765	$6.04e^{-09}$	$2.52e^{-08}$
HALLMARK_ESTROGEN_RESPONSE_LATE	0.184935	0.004802	5.853222	$8.05e^{-09}$	$3.10e^{-08}$
HALLMARK_IL2_STAT5_SIGNALING	0.211812	0.01976	5.527072	$4.92e^{-08}$	$1.76e^{-07}$
EMBRYOGENESIS	0.174955	0.001608	5.297651	$1.67e^{-07}$	$5.55e^{-07}$
HALLMARK_EPITHELIAL_MESENCHYMAL_TRANSITION	0.246368	0.001867	5.190398	$2.90e^{-07}$	$9.07e^{-07}$
HALLMARK_DNA_REPAIR	0.169331	−0.00934	5.002548	$7.50e^{-07}$	$2.21e^{-06}$
HALLMARK_COMPLEMENT	0.204655	0.014286	4.917892	$1.14e^{-06}$	$3.17e^{-06}$
HALLMARK_FATTY_ACID_METABOLISM	−0.175	−0.01994	−4.87811	$1.38e^{-06}$	$3.64e^{-06}$
HALLMARK_PANCREAS_BETA_CELLS	−0.2257	−0.0154	−4.78969	$2.12e^{-06}$	$5.30e^{-06}$
HALLMARK_UNFOLDED_PROTEIN_RESPONSE	−0.14915	−0.01707	−4.48103	$8.95e^{-06}$	$2.13e^{-05}$
HALLMARK_CHOLESTEROL_HOMEOSTASIS	0.148926	−0.00141	4.423661	$1.16e^{-05}$	$2.53e^{-05}$
HALLMARK_INFLAMMATORY_RESPONSE	0.219619	0.022342	4.422877	$1.16e^{-05}$	$2.53e^{-05}$
HALLMARK_E2F_TARGETS	0.182513	−0.00297	4.39443	$1.32e^{-05}$	$2.66e^{-05}$
HALLMARK_IL6_JAK_STAT3_SIGNALING	0.228261	0.010495	4.39235	$1.33e^{-05}$	$2.66e^{-05}$
HALLMARK_KRAS_SIGNALING_UP	0.160773	0.016513	4.008711	$6.90e^{-05}$	0.000133
HALLMARK_APOPTOSIS	0.150887	0.020022	3.910504	0.000103	0.000191
HALLMARK_MYC_TARGETS_V2	0.173592	−0.00647	3.891872	0.000111	0.000198
HALLMARK_PI3K_AKT_MTOR_SIGNALING	0.127265	0.003976	3.820932	0.000147	0.000254
HALLMARK_OXIDATIVE_PHOSPHORYLATION	−0.18948	−0.03356	−3.68458	0.00025	0.000417
HALLMARK_INTERFERON_ALPHA_RESPONSE	0.205442	−0.00389	3.616642	0.000324	0.000523
HALLMARK_ALLOGRAFT_REJECTION	0.193174	0.011578	3.526323	0.000455	0.00071
HALLMARK_MITOTIC_SPINDLE	0.13588	0.010936	3.376937	0.000782	0.001185
HALLMARK_INTERFERON_GAMMA_RESPONSE	0.183761	0.001364	3.302922	0.001015	0.001493
HALLMARK_ADIPOGENESIS	−0.10353	−0.02419	−3.15933	0.001663	0.002376
HALLMARK_ESTROGEN_RESPONSE_EARLY	0.102473	0.003602	3.11537	0.001928	0.002677
HALLMARK_G2M_CHECKPOINT	0.127479	−0.0007	3.092723	0.002078	0.002808
HALLMARK_UV_RESPONSE_UP	0.093472	0.001517	3.072626	0.002221	0.002922
HALLMARK_XENOBIOTIC_METABOLISM	0.088258	0.004748	2.971494	0.003086	0.003956
HALLMARK_REACTIVE_OXYGEN_SPECIES_PATHWAY	−0.09007	−0.00523	−2.37368	0.017935	0.022419
HALLMARK_SPERMATOGENESIS	−0.07121	−0.01352	−2.28486	0.02268	0.027658
HALLMARK_KRAS_SIGNALING_DN	−0.06021	−0.00073	−2.07011	0.038882	0.046288
HALLMARK_ANDROGEN_RESPONSE	−0.08163	0.018995	−2.05748	0.040085	0.04661
HALLMARK_MTORC1_SIGNALING	0.07304	−0.00442	2.02274	0.043556	0.049496

GSVA, Gene Set Variation Analysis. TCGA, the cancer genome atlas. THCA, thyroid cancer.

study showed that caspase 6 is related to favorable prognosis in patients with uterine corpus endometrial cancer [64]. In the context of thyroid cancer, our data indicated that *CASP6* presented significantly differential expression during clinical T stage, N stage, and PFI events, and demonstrated the highest degree of diagnostic efficacy in PRDEGs. After adjusting for multiple COX regression, *CASP6* was selected as the hub gene due to its p-value remaining less than 0.01 and its close association with multiple clinical manifestations. Our findings using IHC revealed that *CASP6* exhibited significant protein-level changes in thyroid cancer compared to normal tissue, suggesting its potential as a diagnostic and prognostic biomarker for thyroid cancer. Furthermore, we noted that *CASP6* may serve as a therapeutic target for inhibitors to reduce PTC recurrence, and its expression level was positively correlated with the tumor burden, indicating its potential as a prognostic biomarker for recognizing high-risk patients. Overall, *CASP6* exhibits potential as both a therapeutic target and a prognostic biomarker in thyroid cancer, although further studies are required to validate its clinical utility.

To better understand the biological function of abnormally expressed genes, GO enrichment analyses showed that the majority of genes participated in necroptotic, apoptotic, and inflammasome complexes, which confirmed that PANoptosis is an extensive and unique crosstalk among several types of PCD pathways. KEGG analysis revealed that *Salmonella* infection (hsa05132) was significantly upregulated. Wu et al. pointed out that *Salmonella* infection could activate the autophagic signaling pathway and downregulate the AKT/mTOR pathway to inhibit anaplastic THCA growth [65]. Recently, abundant evidence has demonstrated that *Salmonella* exerts anti-tumor properties [66] and is synergistic with PANoptosis [67].

In our research, GSEA was implemented on THCA tumor groups, from which significantly enriched pathways were identified, including senescence and autophagy in cancer, the p53 downstream pathway, focal adhesion, and fatty acid omega-oxidation. Mutations in p53 often occur in THCA, especially anaplastic THCA. Research has suggested that transfection of wild-type p53 improves

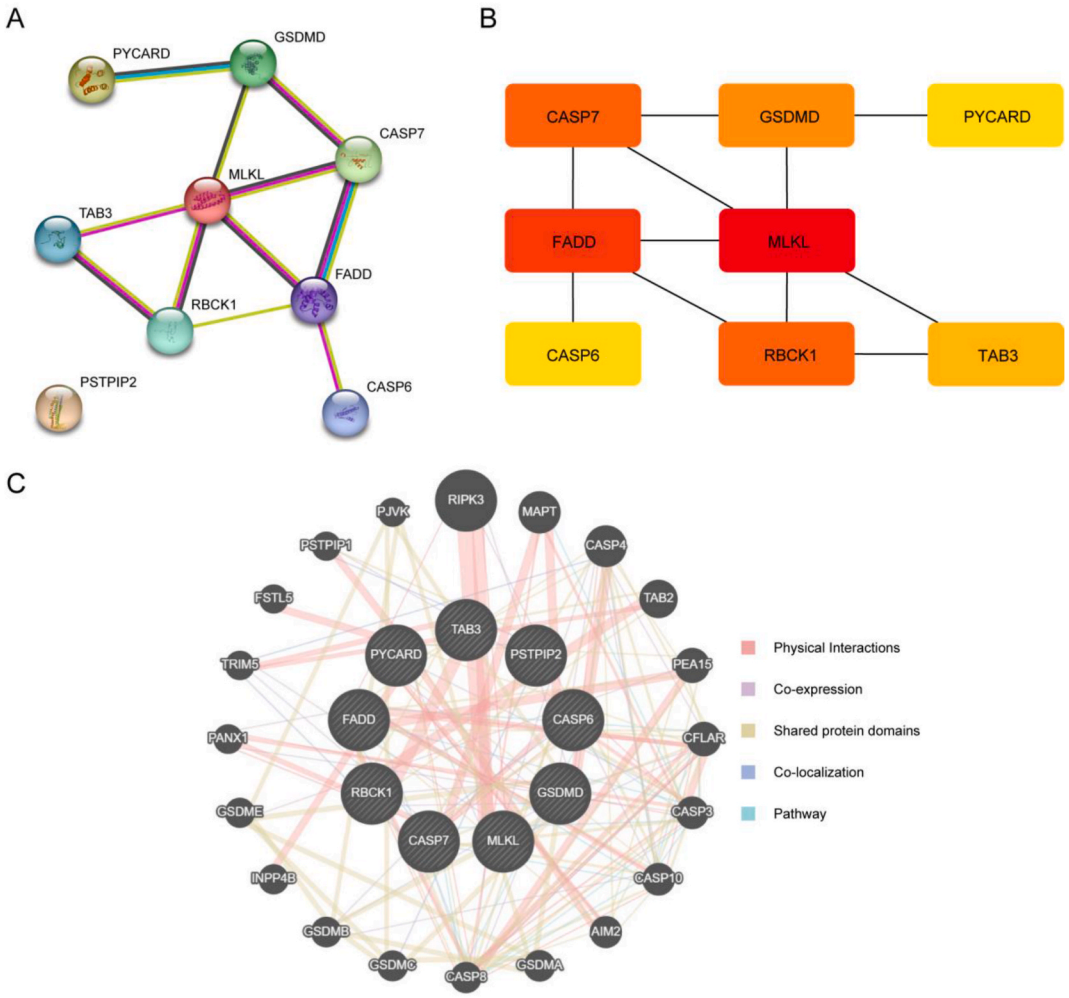

Fig. 6. Protein-protein interaction (PPI) network of PRDEGs. (A) PPI network of PRDEGs constructed with Cytoscape. (B) PPI network of PRDEGs using the MMC method; the rectangle color changes gradually from red to yellow according to the score in descending order. (C) Gene network of PRDEGs produced by GeneMANIA: red line for physical interactions, purple line for co-expression, yellow line for shared protein domain, and blue line for co-localization. PRDEGs, PANoptosis-related differentially expressed genes. PPI, protein-protein interaction. MCC, Maximal Clique Centrality. (For interpretation of the references to color in this figure legend, the reader is referred to the Web version of this article.)

the uptake of radioactive iodine and triggers apoptosis [68,69]. The p53 tumor suppression pathway induces apoptotic cell death and maintains cellular senescence to prevent carcinogenesis. Further, reactivating p53 mutants to restore their tumor-suppressor activity could be a practical anti-tumor approach for TC [70]. Synthesizing our results from GOKEGG enrichment with prior studies, we propose that in the context of thyroid cancer, *CASP6*, a known regulator of PANoptosis, could potentially amplify this process by facilitating PANoptosome assembly and activation, thereby leading to PCD. Simultaneously, *GSDMD* and *MLKL*, implicated in membrane disruption and subsequent pyroptosis and necroptosis, respectively, may serve pivotal roles in cancer cell eradication by promoting inflammatory cell death. Additionally, *RBCK1*, another gene associated with PANoptosis regulation, could significantly influence thyroid cancer progression and PANoptosis modulation. However, these hypotheses warrant further investigation. Future research should prioritize validating the clinical significance of the hub genes in PRDEGs associated with THCA through more extensive studies, creating detection methods, and assessing the therapeutic possibilities to advance precision diagnosis and treatment of THCA.

Although we identified a correlation between PRDEGs expression and prognosis in patients with THCA, several limitations remain to be addressed. First, the data from TCGA and GEO were insufficient, which might have caused selection bias. To validate these assumptions, more experimental data and high-throughput screening results from clinical specimens are acquired to support them. Second, despite the AUC of the model displaying an acceptable discriminative capacity, its performance still needs further

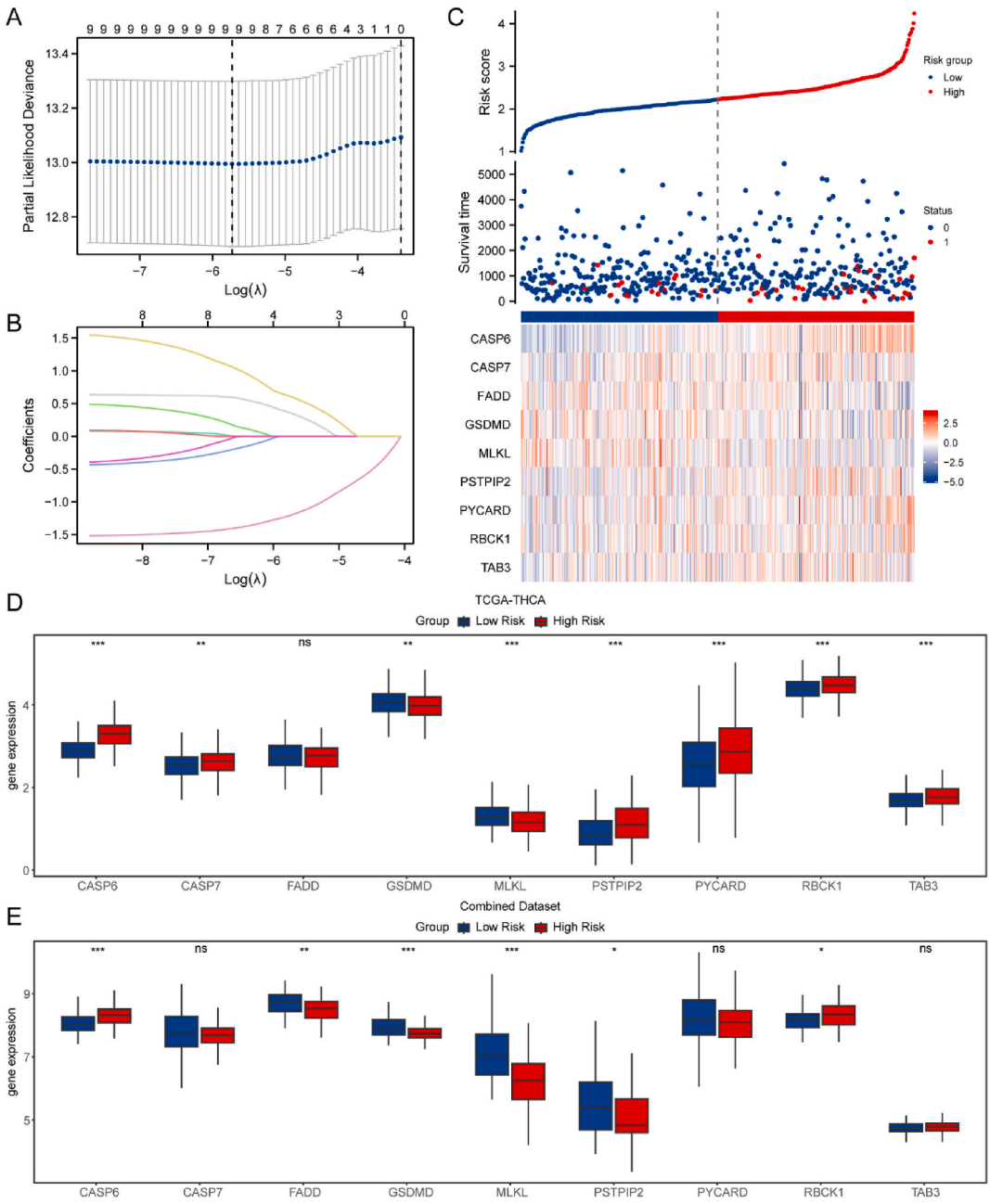

Fig. 7. Risk model of PRDEGs. (A) Ten-time cross-validation for tuning parameter selection in the LASSO model. (B) LASSO coefficient profiles of nine PRDEGs. (C) Risk score curve (upper), showing a gradual increase in the risk score of patients from left to right; point of survival chart (middle), red dot for dead, and blue dot for survival; and survival heap map (lower) of nine candidate PRDEGs in the high- and low-risk groups. (D, E) Boxplot showing distribution patterns of PRDEGs in TCGA-THCA and combined dataset according to the risk score. PRDEGs, PANoptosis-related differentially expressed genes. TCGA, the cancer genome atlas. THCA, thyroid cancer. LASSO, least absolute shrinkage and selection operator. (For interpretation of the references to color in this figure legend, the reader is referred to the Web version of this article.)

improvement. Research with larger sample sizes should be carried out to corroborate and enhance the clinical role of our findings. Third, to elaborate on the biological functions and underlying mechanisms of *CASP6* in THCA, further studies and rigorous *in vivo* and *in vitro* trials should be conducted. Additionally, relying solely on the analysis of a single gene like *CASP6* may limit the comprehensive understanding of the collective impact of PRDEGs on THCA prognosis. Therefore, it is crucial to delve into a broader range of PRDEGs in future research. Finally, as PANoptosis has a close correlation with the immunotherapeutic response of patients with tumors and T cell function in tumor microenvironment [9], we can further investigate the connection of PRDEGs with the tumor immune microenvironment.

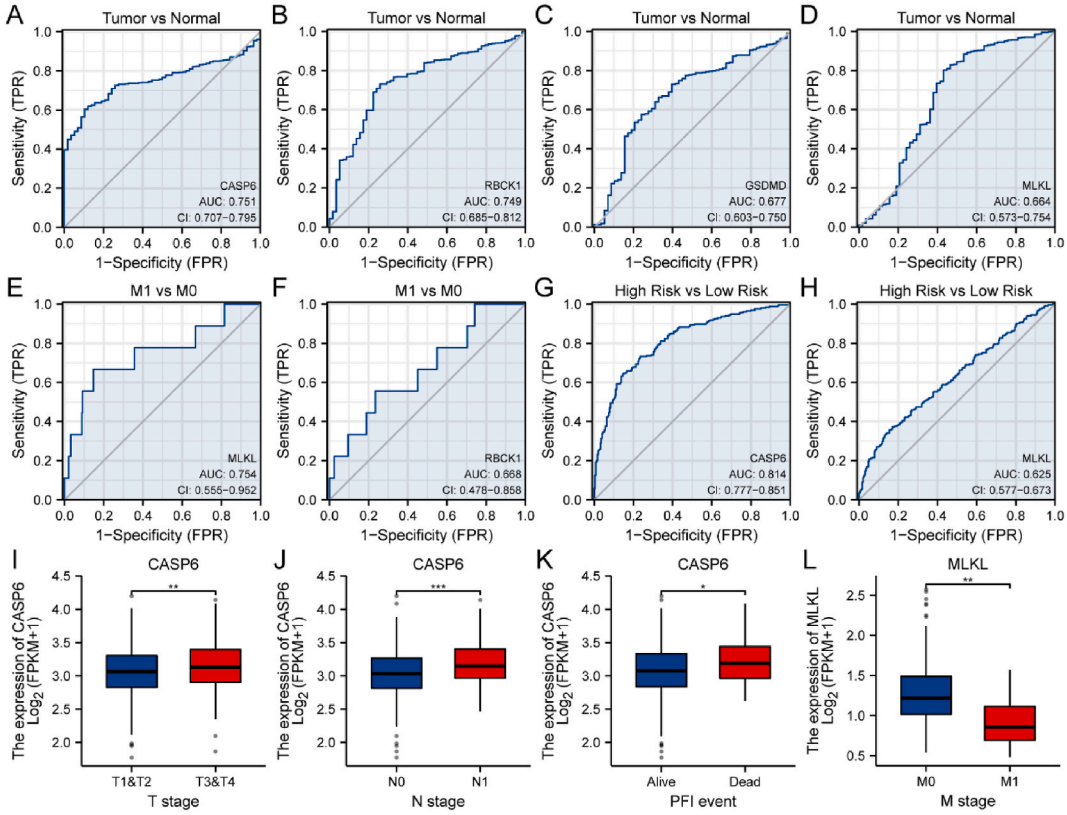

Fig. 8. ROC curves and clinical relevance analyses. (A–D) ROC curves of CASP6 (A), RBCK1 (B), GSDMD (C), and MLKL (D) for diagnosing THCA. (E, F) ROC curve analyses of MLKL (E) and RBCK1 (F) distinguishing the clinical M stage. (G, H) ROC curves of different LASSO risk score in CASP6 (G) and MLKL (H). (I–K) Boxplot display expressions of CASP6 in different clinical parameters: T stage (I), N stage (J), and PFI event (K). (L) Boxplot depicts expression of MLKL according to M stage. *, $P < 0.05$; **, $P < 0.01$; ***, $P < 0.001$. TPR, true positive rate. FPR, false positive rate. ROC, receiver operating characteristic curve. PFI, progression free interval.

6. Conclusions

This study identified nine PRDEGs (*CASP6*, *CASP7*, *FADD*, *GSDMD*, *MLKL*, *PSTPIP2*, *PYCARD*, *RBCK1*, and *TAB3*) for the first time that may be used as novel prognostic models for predicting THCA risks. Moreover, our results showed that a nomogram model including *CASP6*, *MLKL*, and *RBCK1* may be closely related to the survival probability of THCA. Furthermore, among the identified PRDEGs, *CASP6* levels were considerably correlated with the prognosis of patients with THCA, which provided a new treatment direction. However, the specific mechanisms by which PRGs regulate tumorigenesis and the advancement of THCA warrant further investigation.

Availability of data and materials

TCGA (https://portal.gdc.cancer.gov/), UCSC Xena database (http://genome.ucsc.edu), GEO (https://www.ncbi.nlm.nih.gov/geo/), Genecards (https://www.genecards.org/), MSigDB database (http://software.broadinstitute.org/gsea/msigdb), STRING (https://string-db.org/), GeneMANIA (http://apps.cytoscape.org/apps/genemania), HPA website (https://www.proteinatlas.org/).

Ethics declarations

Our data are sourced from open public databases. Informed consent was obtained from all patients prior to their participation. The study protocol was approved by the institutional ethics committee, and all procedures were conducted in compliance with the ethical standards outlined in the Declaration of Helsinki.

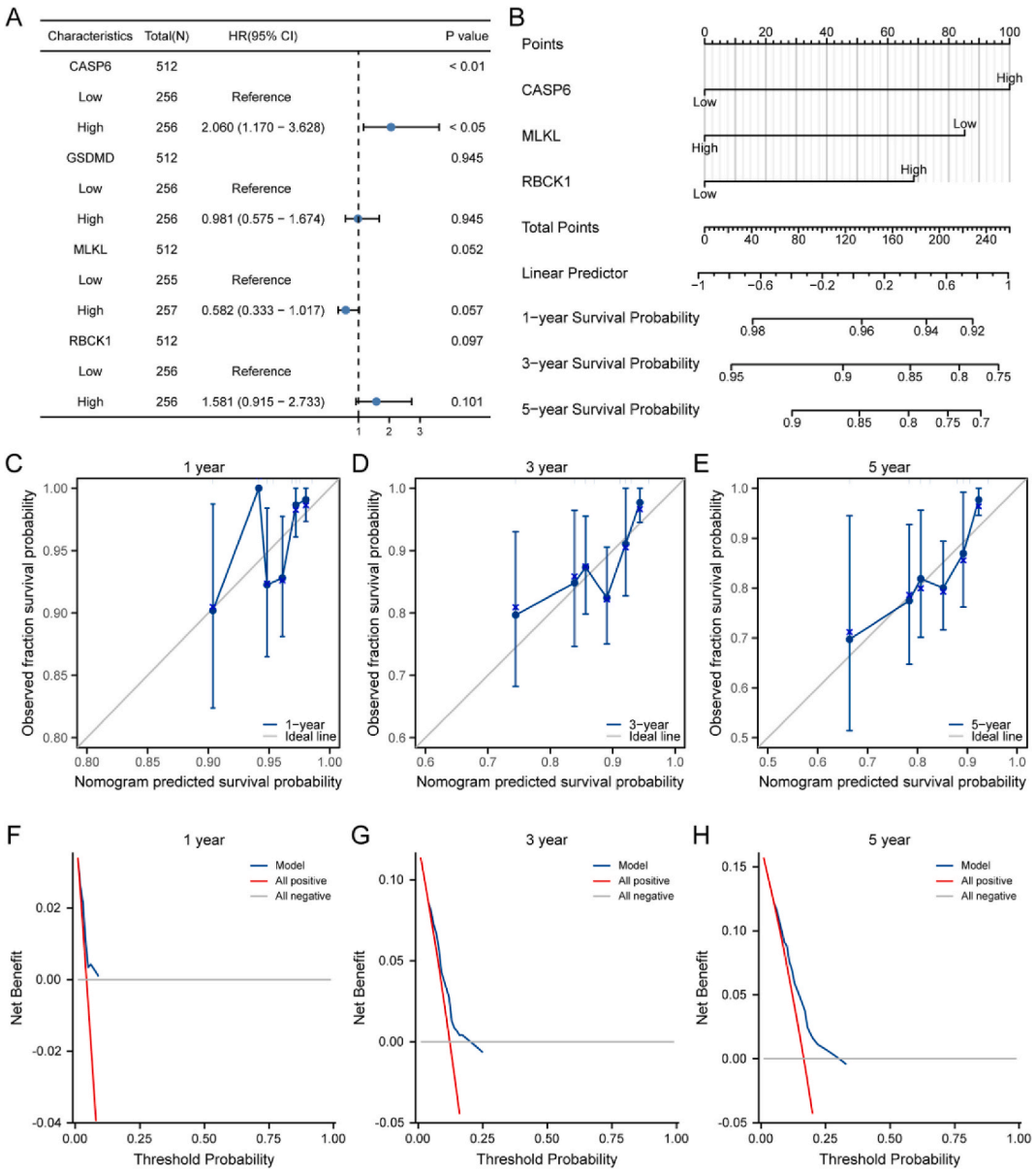

Fig. 9. Cox regression model. (A) Forest plot of multivariate Cox analysis. (B) Prognostic nomogram for the 1-, 3-, and 5-year survival probability of patients with THCA. (*C*–E) Nomogram calibration curves for predicting the 1-, 3-, and 5-year survival probability of TCGA-THCA cohort. The x-axis is the predicted survival probability and the y-axis is the observed fraction survival probability. (F–H) DCA for LASSO-Cox regression model in the 1-, 3-, and 5-year predictions. The x-axis is the risk threshold probability that changes from 0 to 1 (right truncated at 1.00) and the y-axis is the calculated net benefit for a given threshold probability. The blue curve depicts the net benefit of the risk model, whereas the red and gray lines display the net benefits in the alternative strategies of all positive (red) versus negative (gray) in the dataset. DCA, decision curve analysis. LASSO, least absolute shrinkage and selection operator. (For interpretation of the references to color in this figure legend, the reader is referred to the Web version of this article.)

Data availability statement

This study analyzed publicly accessible datasets, which include The Cancer Genome Atlas (TCGA, https://tcga-data.nci.nih.gov/tcga/), the UCSC Xena database (http://genome.ucsc.edu), and the GSE33630, GSE35570, GSE65144, and GSE76039 datasets from the Gene Expression Omnibus (GEO, https://www.ncbi.nlm.nih.gov/geo/query).

Table 7
Cox regression to identify hub genes and clinical features associated with PFI.

Characteristics	Total (N)	Univariate analysis		Multivariate analysis	
		HR (95 % CI)	*p*-value	HR (95 % CI)	*P*-value
CASP6	512		<0.01		
Low	256	Reference		Reference	
High	256	2.060 (1.170–3.628)	<0.05	2.132 (1.209–3.759)	<0.01
GSDMD	512		0.945		
Low	256	Reference			
High	256	0.981 (0.575–1.674)	0.945		
MLKL	512		0.052		
Low	255	Reference		Reference	
High	257	0.582 (0.333–1.017)	0.057	0.524 (0.299–0.921)	<0.05
RBCK1	512		0.097		
Low	256	Reference		Reference	
High	256	1.581 (0.915–2.733)	0.101	1.680 (0.969–2.914)	0.065

PFI, progression free interval. HR, hazard ratio. CI, confidence interval.

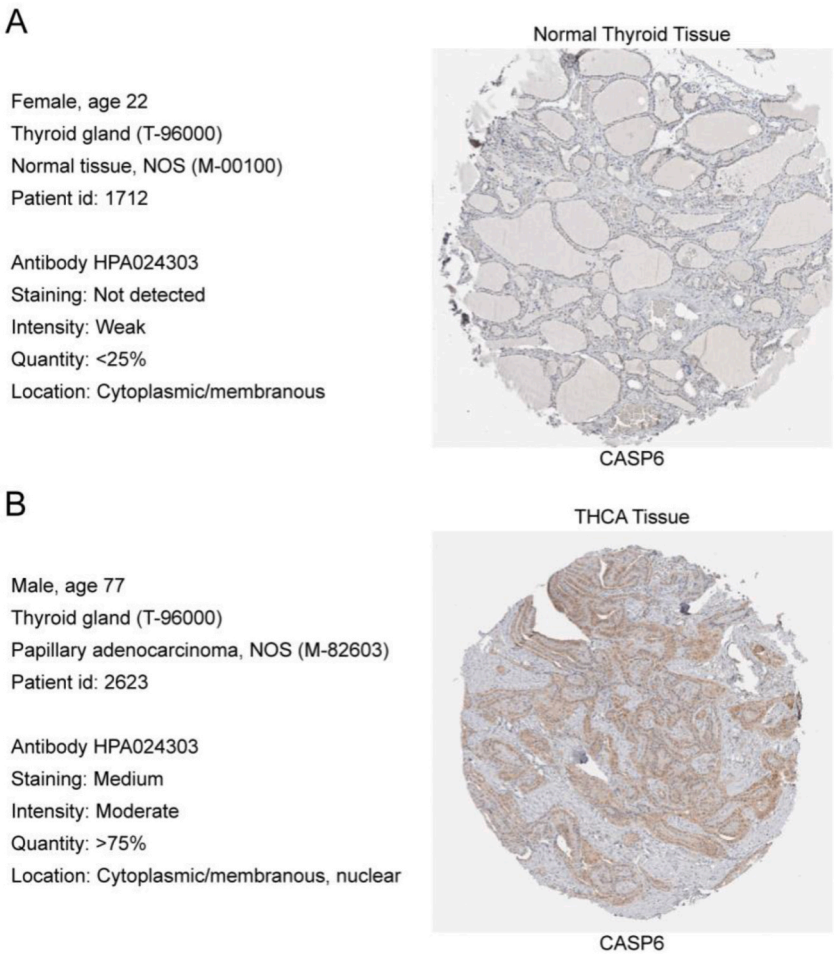

Fig. 10. CASP6 expression levels Normal thyroid (A) and THCA (B) tissues shown by immunohistochemistry (IHC) from the human protein atlas. THCA, thyroid cancer.

CRediT authorship contribution statement

Diya Xie: Writing – original draft, Software, Methodology, Formal analysis. **Liyong Huang:** Writing – review & editing, Visualization, Validation, Conceptualization. **Cheng Li:** Formal analysis, Data curation. **Ruozhen Wu:** Software, Formal analysis, Data curation. **Zhigang Zheng:** Visualization. **Fengmin Liu:** Validation, Formal analysis, Data curation. **Huayong Cheng:** Visualization.

Declaration of competing interest

The authors declare that they have no known competing financial interests or personal relationships that could have appeared to influence the work reported in this paper.

Acknowledgments

We wish to acknowledge B. Xie and Y.H. Xiao, who have provided critical advice on the revision process of our manuscript, and be thankful for H.W. Xie, whose companionship always makes us vigorous.

Appendix A. Supplementary data

Supplementary data to this article can be found online at https://doi.org/10.1016/j.heliyon.2024.e31707.

References

[1] B. Wang, et al., Research on a Weighted Gene Co-expression Network Analysis method for mining pathogenic genes in thyroid cancer, PLoS One 17 (8) (2022) e0272403, https://doi.org/10.1371/journal.pone.0272403.
[2] J. Kim, J.E. Gosnell, S.A. Roman, Geographic influences in the global rise of thyroid cancer, Nat. Rev. Endocrinol. 16 (1) (2020) 17–29, https://doi.org/10.1038/s41574-019-0263-x.
[3] G.E. Naoum, et al., Novel targeted therapies and immunotherapy for advanced thyroid cancers, Mol. Cancer 17 (1) (2018) 51, https://doi.org/10.1186/s12943-018-0786-0.
[4] L. Yip, J.A. Sosa, Molecular-directed treatment of differentiated thyroid cancer: advances in diagnosis and treatment, JAMA Surg 151 (7) (2016) 663–670, https://doi.org/10.1001/jamasurg.2016.0825.
[5] X. Fu, et al., TFAP2B overexpression contributes to tumor growth and progression of thyroid cancer through the COX-2 signaling pathway, Cell Death Dis. 10 (6) (2019) 397, https://doi.org/10.1038/s41419-019-1600-7.
[6] C.F. Eustatia-Rutten, et al., Survival and death causes in differentiated thyroid carcinoma, J. Clin. Endocrinol. Metab. 91 (1) (2006) 313–319, https://doi.org/10.1210/jc.2005-1322.
[7] S. Fuloria, et al., Comprehensive review of methodology to detect reactive oxygen species (ROS) in mammalian species and establish its relationship with antioxidants and cancer, Antioxidants 10 (1) (2021), https://doi.org/10.3390/antiox10010128.
[8] W.T. Yan, et al., PANoptosis-like cell death in ischemia/reperfusion injury of retinal neurons, Neural Regen Res 18 (2) (2023) 357–363, https://doi.org/10.4103/1673-5374.346545.
[9] R. Karki, et al., Interferon regulatory factor 1 regulates PANoptosis to prevent colorectal cancer, JCI Insight 5 (12) (2020), https://doi.org/10.1172/jci.insight.136720.
[10] R. Karki, et al., ADAR1 restricts ZBP1-mediated immune response and PANoptosis to promote tumorigenesis, Cell Rep. 37 (3) (2021) 109858, https://doi.org/10.1016/j.celrep.2021.109858.
[11] A. Colaprico, et al., TCGAbiolinks: an R/Bioconductor package for integrative analysis of TCGA data, Nucleic Acids Res. 44 (8) (2016) e71, https://doi.org/10.1093/nar/gkv1507.
[12] M.J. Goldman, et al., Visualizing and interpreting cancer genomics data via the Xena platform, Nat. Biotechnol. 38 (6) (2020) 675–678, https://doi.org/10.1038/s41587-020-0546-8.
[13] M.E. Ritchie, et al., Limma powers differential expression analyses for RNA-sequencing and microarray studies, Nucleic Acids Res. 43 (7) (2015) e47, https://doi.org/10.1093/nar/gkv007.
[14] G. Tomas, et al., A general method to derive robust organ-specific gene expression-based differentiation indices: application to thyroid cancer diagnostic, Oncogene 31 (41) (2012) 4490–4498, https://doi.org/10.1038/onc.2011.626.
[15] G. Dom, et al., A gene expression signature distinguishes normal tissues of sporadic and radiation-induced papillary thyroid carcinomas, Br. J. Cancer 107 (6) (2012) 994–1000, https://doi.org/10.1038/bjc.2012.302.
[16] D. Handkiewicz-Junak, et al., Gene signature of the post-Chernobyl papillary thyroid cancer, Eur. J. Nucl. Med. Mol. Imag. 43 (7) (2016) 1267–1277, https://doi.org/10.1007/s00259-015-3303-3.
[17] C.A. von Roemeling, et al., Aberrant lipid metabolism in anaplastic thyroid carcinoma reveals stearoyl CoA desaturase 1 as a novel therapeutic target, J. Clin. Endocrinol. Metab. 100 (5) (2015) E697–E709, https://doi.org/10.1210/jc.2014-2764.
[18] I. Landa, et al., Genomic and transcriptomic hallmarks of poorly differentiated and anaplastic thyroid cancers, J. Clin. Invest. 126 (3) (2016) 1052–1066, https://doi.org/10.1172/JCI85271.
[19] S. Davis, P.S. Meltzer, GEOquery: a bridge between the gene expression Omnibus (GEO) and BioConductor, Bioinformatics 23 (14) (2007) 1846–1847, https://doi.org/10.1093/bioinformatics/btm254.
[20] G. Tomás, et al., A general method to derive robust organ-specific gene expression-based differentiation indices: application to thyroid cancer diagnostic 31 (41) (2012) 4490–4498.
[21] G. Dom, et al., A gene expression signature distinguishes normal tissues of sporadic and radiation-induced papillary thyroid carcinomas 107 (6) (2012) 994–1000.
[22] I. Landa, et al., Genomic and transcriptomic hallmarks of poorly differentiated and anaplastic thyroid cancers 126 (3) (2016) 1052–1066.
[23] G. Stelzer, et al., The GeneCards suite: from gene data mining to disease genome sequence analyses, Curr Protoc Bioinformatics 54 (2016) 1 30 1–1 30 33, https://doi.org/10.1002/cpbi.5.
[24] J. Huang, et al., Analysis of PANoptosis-related LncRNA-miRNA-mRNA network reveals LncRNA SNHG7 involved in chemo-resistance in colon adenocarcinoma, Front. Oncol. 12 (2022) 888105, https://doi.org/10.3389/fonc.2022.888105.
[25] X. Wang, et al., PANoptosis-based molecular clustering and prognostic signature predicts patient survival and immune landscape in colon cancer, Front. Genet. 13 (2022) 955355, https://doi.org/10.3389/fgene.2022.955355.
[26] C. Gene Ontology, Gene Ontology consortium: going forward, Nucleic Acids Res. 43 (Database issue) (2015) D1049–D1056, https://doi.org/10.1093/nar/gku1179.
[27] M. Kanehisa, S. Goto, KEGG: kyoto encyclopedia of genes and genomes, Nucleic Acids Res. 28 (1) (2000) 27–30, https://doi.org/10.1093/nar/28.1.27.
[28] V. Subramaniyan, et al., A review on epidermal growth factor receptor's role in breast and non-small cell lung cancer, Chem. Biol. Interact. 351 (2022) 109735, https://doi.org/10.1016/j.cbi.2021.109735.
[29] S. Hanzelmann, R. Castelo, J. Guinney, GSVA: gene set variation analysis for microarray and RNA-seq data, BMC Bioinf. 14 (2013) 7, https://doi.org/10.1186/1471-2105-14-7.

[30] D. Szklarczyk, et al., STRING v11: protein-protein association networks with increased coverage, supporting functional discovery in genome-wide experimental datasets, Nucleic Acids Res. 47 (D1) (2019) D607–D613, https://doi.org/10.1093/nar/gky1131.

[31] P. Shannon, et al., Cytoscape: a software environment for integrated models of biomolecular interaction networks, Genome Res. 13 (11) (2003) 2498–2504, https://doi.org/10.1101/gr.1239303.

[32] R. Tibshirani, The lasso method for variable selection in the Cox model, Stat. Med. 16 (4) (1997) 385–395, https://doi.org/10.1002/(sici)1097-0258(19970228)16:4<385::aid-sim380>3.0.co;2-395.

[33] S. Ramli, et al., Long noncoding RNA UCA1 in gastrointestinal cancers: molecular regulatory roles and patterns, mechanisms, and interactions, JAMA Oncol. 2021 (2021) 5519720, https://doi.org/10.1155/2021/5519720.

[34] T. Tataranni, C. Piccoli, Dichloroacetate (DCA) and cancer: an overview towards clinical applications, Oxid. Med. Cell. Longev. 2019 (2019) 8201079, https://doi.org/10.1155/2019/8201079.

[35] K. Colwill, G. Renewable Protein Binder Working, S. Graslund, A roadmap to generate renewable protein binders to the human proteome, Nat. Methods 8 (7) (2011) 551–558, https://doi.org/10.1038/nmeth.1607.

[36] S. Engebretsen, J. Bohlin, Statistical predictions with glmnet, Clin. Epigenet. 11 (1) (2019) 123, https://doi.org/10.1186/s13148-019-0730-1.

[37] J.N. Mandrekar, Receiver operating characteristic curve in diagnostic test assessment, J. Thorac. Oncol. 5 (9) (2010) 1315–1316, https://doi.org/10.1097/JTO.0b013e3181ec173d.

[38] S.I. Sherman, Thyroid carcinoma, Lancet 361 (9356) (2003) 501–511, https://doi.org/10.1016/s0140-6736(03)12488-9.

[39] R. Thapa, et al., Unveiling the connection: long-chain non-coding RNAs and critical signaling pathways in breast cancer, Pathol. Res. Pract. 249 (2023) 154736, https://doi.org/10.1016/j.prp.2023.154736.

[40] S.E. Wobker, et al., Use of BRAF v600e immunocytochemistry on FNA direct smears of papillary thyroid carcinoma, Cancer Cytopathol 123 (9) (2015) 531–539, https://doi.org/10.1002/cncy.21575.

[41] S. Christgen, et al., Identification of the PANoptosome: a molecular platform triggering pyroptosis, apoptosis, and necroptosis (PANoptosis), Front. Cell. Infect. Microbiol. 10 (2020) 237, https://doi.org/10.3389/fcimb.2020.00237.

[42] N. Pandian, T.D. Kanneganti, PANoptosis: a unique innate immune inflammatory cell death modality, J. Immunol. 209 (9) (2022) 1625–1633, https://doi.org/10.4049/jimmunol.2200508.

[43] H. Pan, et al., Characterization of PANoptosis patterns predicts survival and immunotherapy response in gastric cancer, Clin. Immunol. 238 (2022) 109019, https://doi.org/10.1016/j.clim.2022.109019.

[44] J. Zhao, et al., TAB3 promotes human esophageal squamous cell carcinoma proliferation and invasion via the NF-kappaB pathway, Oncol. Rep. 40 (5) (2018) 2876–2885, https://doi.org/10.3892/or.2018.6686.

[45] A. Criollo, et al., Inhibition of autophagy by TAB2 and TAB3, EMBO J. 30 (24) (2011) 4908–4920, https://doi.org/10.1038/emboj.2011.413.

[46] R.K.S. Malireddi, et al., Innate immune priming in the absence of TAK1 drives RIPK1 kinase activity-independent pyroptosis, apoptosis, necroptosis, and inflammatory disease, J. Exp. Med. 217 (3) (2020), https://doi.org/10.1084/jem.20191644.

[47] P. Orning, et al., Pathogen blockade of TAK1 triggers caspase-8-dependent cleavage of gasdermin D and cell death, Science 362 (6418) (2018) 1064–1069, https://doi.org/10.1126/science.aau2818.

[48] T. Delanghe, Y. Dondelinger, M.J.M. Bertrand, RIPK1 kinase-dependent death: a symphony of phosphorylation events, Trends Cell Biol. 30 (3) (2020) 189–200, https://doi.org/10.1016/j.tcb.2019.12.009.

[49] F. Anson, S. Thayumanavan, J.A. Hardy, Exogenous introduction of initiator and executioner caspases results in different apoptotic outcomes, JACS Au 1 (8) (2021) 1240–1256, https://doi.org/10.1021/jacsau.1c00261.

[50] V. Chitu, et al., The PCH family member MAYP/PSTPIP2 directly regulates F-actin bundling and enhances filopodia formation and motility in macrophages, Mol. Biol. Cell 16 (6) (2005) 2947–2959, https://doi.org/10.1091/mbc.e04-10-0914.

[51] S. Mukherjee, et al., Unlocking exosome-based theragnostic signatures: deciphering secrets of ovarian cancer metastasis, ACS Omega 8 (40) (2023) 36614–36627, https://doi.org/10.1021/acsomega.3c02837.

[52] R. Zhou, et al., A role for mitochondria in NLRP3 inflammasome activation, Nature 469 (7329) (2011) 221–225, https://doi.org/10.1038/nature09663.

[53] P. Broz, P. Pelegrin, F. Shao, The gasdermins, a protein family executing cell death and inflammation, Nat. Rev. Immunol. 20 (3) (2020) 143–157, https://doi.org/10.1038/s41577-019-0228-2.

[54] E.O. Machida, et al., Hypermethylation of ASC/TMS1 is a sputum marker for late-stage lung cancer, Cancer Res. 66 (12) (2006) 6210–6218, https://doi.org/10.1158/0008-5472.CAN-05-4447.

[55] L. Wu, et al., Methylation of ASC/TMS1 promoter is associated with poor prognosis of patients with gastric cancer, Clin. Transl. Oncol. 18 (3) (2016) 296–303, https://doi.org/10.1007/s12094-015-1367-y.

[56] E. Brunetto, et al., The IL-1/IL-1 receptor axis and tumor cell released inflammasome adaptor ASC are key regulators of TSLP secretion by cancer associated fibroblasts in pancreatic cancer, J Immunother Cancer 7 (1) (2019) 45, https://doi.org/10.1186/s40425-019-0521-4.

[57] N. Gustafsson Sheppard, N. Heldring, K. Dahlman-Wright, Estrogen receptor-alpha, RBCK1, and protein kinase C beta 1 cooperate to regulate estrogen receptor-alpha gene expression, J. Mol. Endocrinol. 49 (3) (2012) 277–287, https://doi.org/10.1530/JME-12-0073.

[58] F.A. Rizwi, et al., Janus kinase-signal transducer and activator of transcription inhibitors for the treatment and management of cancer, J. Environ. Pathol. Toxicol. Oncol. 42 (4) (2023) 15–29, https://doi.org/10.1615/JEnvironPatholToxicolOncol.2023045403.

[59] C. Donley, et al., Identification of RBCK1 as a novel regulator of FKBPL: implications for tumor growth and response to tamoxifen, Oncogene 33 (26) (2014) 3441–3450, https://doi.org/10.1038/onc.2013.306.

[60] T. Di Matola, et al., Lovastatin-induced apoptosis in thyroid cells: involvement of cytochrome c and lamin B, Eur. J. Endocrinol. 145 (5) (2001) 645–650, https://doi.org/10.1530/eje.0.1450645.

[61] M. Zheng, et al., Caspase-6 is a key regulator of innate immunity, inflammasome activation, and host defense, Cell 181 (3) (2020) 674–687 e13, https://doi.org/10.1016/j.cell.2020.03.040.

[62] B. Chao, et al., Predicting the prognosis of glioma by pyroptosis-related signature, J. Cell Mol. Med. 26 (1) (2022) 133–143, https://doi.org/10.1111/jcmm.17061.

[63] D.S. Simpson, et al., Interferon-gamma primes macrophages for pathogen ligand-induced killing via a caspase-8 and mitochondrial cell death pathway, Immunity 55 (3) (2022) 423–441, https://doi.org/10.1016/j.immuni.2022.01.003.

[64] Q. Liu, M. Yu, T. Zhang, Construction of oxidative stress-related genes risk model predicts the prognosis of uterine corpus endometrial cancer patients, Cancers 14 (22) (2022), https://doi.org/10.3390/cancers14225572.

[65] L.H. Wu, C.R. Pangilinan, C.H. Lee, Downregulation of AKT/mTOR signaling pathway for Salmonella-mediated autophagy in human anaplastic thyroid cancer, J. Cancer 13 (11) (2022) 3268–3279, https://doi.org/10.7150/jca.75163.

[66] B.H. Al-Saafeen, M.J. Fernandez-Cabezudo, B.K. Al-Ramadi, Integration of Salmonella into combination cancer therapy, Cancers 13 (13) (2021), https://doi.org/10.3390/cancers13133228.

[67] F. Badie, et al., Use of Salmonella bacteria in cancer therapy: direct, drug delivery and combination approaches, Front. Oncol. 11 (2021) 624759, https://doi.org/10.3389/fonc.2021.624759.

[68] L. Liu, et al., Wild-type P53 induces sodium/iodide symporter expression allowing radioiodide therapy in anaplastic thyroid cancer, Cell. Physiol. Biochem. 43 (3) (2017) 905–914, https://doi.org/10.1159/000481640.

[69] N. Mujafarkani, et al., Unveiling a novel terpolymer-metal complex: a detailed exploration of synthesis, characterization, and its potential as an antimicrobial and antioxidant agent, Heliyon 9 (10) (2023) e20459, https://doi.org/10.1016/j.heliyon.2023.e20459.

[70] R.L. Messina, et al., Reactivation of p53 mutants by prima-1 [corrected] in thyroid cancer cells, Int. J. Cancer 130 (10) (2012) 2259–2270, https://doi.org/10.1002/ijc.26228.